Scaling analyses of a SB-LOCA counterpart test between BETHSY and LSTF facilities and a three loops PWR

Antoine Ciechocki, Sofia Carnevali, Dominique Bestion, Lionel Rossi

Scaling analyses of a SB-LOCA counterpart test between BETHSY and LSTF facilities and a three loops PWR

Antoine Ciechocki [a,*], Sofia Carnevali [a], Dominique Bestion [b], Lionel Rossi [c]

[a] *Université Paris-Saclay, CEA, Service de Thermo-hydraulique et de Mécanique des Fluides, 91191, Gif-sur-Yvette, France*
[b] *22 Avenue de l'Europe, 38120, Saint Egrève, France*
[c] *CEA Cadarache, Service de Technologie des Composants et des Procédés, 13115, Saint-Paul-lez-Durance, France*

Abstract

The objective of this work is to revisit the scaling analysis of a 6% Cold Leg break LOCA transient of a pressurized water reactor (PWR) using the results of a counterpart test and the support of post-test calculations with a system code. The 6.2-TC and SB-CL-21 tests performed respectively on the French BETHSY facility and the Japanese LSTF-ROSA-IV facility are analyzed. Experimental and calculated results are presented. A comparison is made with the simulation results of a commercial PWR. The transient is divided into five phases and important bifurcating events are identified. In the present work, a phenomenological analysis of the transient is conducted. The Fractional Scaling Analysis (FSA) methodology is applied at system and component scales by writing mass and pressure equations for the whole primary system and for the pressurizer. The CATHARE system thermal hydraulic code is used to estimate the effect metrics specific to this method. The relative weight of the processes that control the mass and pressure are evaluated. Some conclusions are drawn on the presence of possible distortions between the transients in the facilities and in the full-scale reactor. The key point of this study is to show the applicability of a modern top-down approach scaling method, supported by code calculations at different scales.

Keywords: Scaling, FSA, SB-LOCA, Counterpart Test, BETHSY, LSTF

* Corresponding author.
Email addresses: antoine.ciechocki@cea.fr (Antoine Ciechocki), sofia.carnevali@cea.fr (Sofia Carnevali), dominique.bestion@wanadoo.fr (Dominique Bestion), lionel.rossi@cea.fr (Lionel Rossi)

1. Introduction

In order to simulate the thermal hydraulic behaviour of nuclear reactor accidental transients, scaling analyses must be performed (see Bestion et al., 2017). Since a full-scale experimental reactor is not affordable, experimental facilities are needed to simulate reactor transients. Reduced-scale tests are performed to understand the phenomena occurring during transients. Scaling methods are used to design scaled-down reactor models and to define test conditions that represent with minimal distortions the processes that would take place during the full-scale reactor transient. These scaling methods define design criteria to respect important phenomena having an impact on the Figure of Merit (FoM) of the transient. In the design and scaling of the facilities, important processes are identified during the Phenomena Identification and Ranking Table (PIRT) (Wilson and Boyack, 1998). The results of the experimental tests are used to support the validation of the numerical simulation tools. Codes can then assist PIRT and scaling analysis.

Scaling analysis can also be used to make recommendations for improving code models in order to better describe some dominant transient processes. The code validation compares the code predictions with experimental data. Code aims to correctly predict the effects of dominant and influent processes to be able to do the transposition to the full-scale reactor transient. This is called the "code scalability" or code capability to do the "scaling-up". During a scaling analysis, a code is not yet perfectly predictive. This remains ideal until a full validation proves its scalability. However, current system codes have a good maturity since they have been extensively validated.
The SB-LOCA transient is a nuclear safety Design-Basis Accident (DBA) whose interest stems from the Three Miles Island (TMI) accident. This primary system coolant leakage scenario shifted the focus from LB-LOCA to SB-LOCA. This work revisits a posteriori the phenomenology and the scaling of rather old integral tests using the current knowledge and tools. A 6% Small-Break Loss Of Coolant Accident (SB-LOCA) is analysed using a counterpart test performed on two ITFs (D'Auria et al., 1992; Kumamaru et al., 1992) and a reference reactor transient simulation:

- The 6.2-TC test performed on the French BETHSY facility (Equipe BETHSY, 1990).
- The SB-CL-21 test performed on the Japanese LSTF-ROSA-IV facility (The ROSA-V Group, 1985).
- A full-scale model of a Framatome commercial Pressurized Water Reactor (PWR), which is the reference reactor of the BETHSY facility.

Both Integral Test Facilities (ITF) are scaled based on respecting power-to-volume ratio (Nahavandi et al., 1979) and respecting Full-Height Full-Pressure (FHFP) of their reference reactor.

Experimental data are compared to predictions of the CATHARE thermal hydraulic system code (Bestion, 1990; Emonot et al., 2011; Préa et al., 2020). An objective is to identify and quantify system scale distortions between the two facilities and the reactor and to discuss design choices.

The scaling analysis in this study uses the Fractional Scaling Analysis (FSA) methodology (Zuber et al., 2007), which is an improvement of the Hierarchical Two Tiered Scaling (H2TS) method (Zuber, 1991). They are both intended for scale transposition and to support system codes. The FSA and H2TS methods are based on the concepts of hierarchy and scaling groups. They introduce the concepts of top-down approach followed by the bottom-up approach. The top-down step starts the scaling analysis at the global system scale to define scaling ratios for global parameters such as volume and power. The scaling analysis then divides the whole system into individual parts and considering progressively smaller scales, i.e. the component scale, the sub-component scale, to the local process scale. The bottom-up step is the reverse process, which bring together individual information, from basic building blocks to the complex system. This is a comprehensive method for the scaling analysis in the field of nuclear reactor transients. It also provides efficiency through cost-effective and timely resolution (Zuber et al., 1998). However, advanced methods such as H2TS and FSA require a high level of expertise in transient analysis and a deep understanding of two-phase thermal hydraulics. No handbook for scaling method exists and guidance on how to apply them is required (Ciechocki et al., 2022). This work intends to see how system codes can support the scaling analysis based on the application of the FSA.

Nomenclature

A	Area (m^2)
e	Specific internal energy (J/kg)
h	Local specific enthalpy (J/kg)
$\vec{F}$	Force vector (N)
H	Volume averaged specific enthalpy (J/kg)
K	Global expansion coefficient (m^3/Pa)
M	Mass (kg)
$\dot{M}$	Mass flow rate (kg/s)
$\vec{n}$	Unit normal vector (-)
p	Local pressure (Pa)
P	Pressure in a control volume (Pa)
$\dot{P}$	Rate of pressure change (Pa/s)
q	Power source (W)
Q	Volume Rate of Change or volume flow rate (m^3/s)
t	Time (s)
T	Temperature (°C)
$\bar{\bar{T}}$	Stress tensor (N/m^2)
u	Velocity (m/s)
V	Control volume (m^3)
Y	Thermophysical property
W	Power (W)
γ	Expansion coefficient (-)
μ_k	$- v'_{k,p} - v_k \cdot v'_{k,h}$ ($m^4.s^2/kg^2$)
v	Specific volume (m^3/kg)
$v'_{k,p}$	Partial derivative of specific volume of phase k with respect to pressure ($m^4.s^2/kg^2$)
$v'_{k,h}$	Partial derivative of specific volume of phase k with respect to enthalpy ($m.s^2$/kg)
Π	Characteristic time ratio (-)
ρ	Density (kg/m^3)
ϖ	$\frac{H_v - H_l}{v_v - v_l}$ (J/m^3)
τ	Residence time (s)
ϕ	Agent of Change (-)
ω	Fractional Rate of Change (s^{-1})
Ω	Effect metric (-)

Subscripts

0	Initial/reference value
1	Related to primary system
acc.	Related to accumulator
break	Related to the break
core	Related to the core
ext.	External (source)
f	Related to fluid boundary
i	Related to interface
in	Inlet
k	Related to the phase *k*
l	Related to liquid phase
out	Outlet
ov	Related to other volumes
ow	Related to other walls
prz	Related to pressurizer
s	Saturation conditions
SG	Related to steam generators

Acronyms

AFW	Auxiliary Feedwater
AIS	Accumulator Injection System
SBD	Subcooled BlowDown
BETHSY	"Boucle d'Etude ThermoHydraulique SYstème"
CATHARE	"Code Avancé de THermohydraulique pour les Accidents de Réacteurs à Eau"
CEA	"Commissariat à l'Énergie Atomique et aux énergies alternatives"
CL	Cold Leg
DBA	Design-Basis Accident
EDF	"Électricité de France"
EXP.	Experimental results
FoM	Figure of Merit
FHFP	Full-Height Full-Pressure
FRC	Fractional Rate of Change
FSA	Fractional Scaling Analysis
H2TS	Hierarchical Two Tiered Scaling
HQMD	High-Quality Mixture Discharge
HL	Hot Leg
HPIS	High Pressure Injection System
IET	Integral Effect Test
IL	Intermediate Leg
ITF	Integral Test Facility
JAERI	Japan Atomic Energy Research Institute
LB-LOCA	Large-Break Loss Of Coolant Accident
SB-LOCA	Small-Break Loss Of Coolant Accident
LSC	Loop Seal Clearing
LSP	Loop Seal Plugging
LSTF	Large Scale Test Facility
NEA	Nuclear Energy Agency
NC	Natural Circulation
OECD	Organisation for Economic Co-operation and Development
PCT	Peak Clad Temperature
PIRT	Phenomena Identification and Ranking Table
PoI	Parameter of Interest
PRZ	Pressurizer
PWR	Pressurized Water Reactor
RCM	Reflux Condenser Mode
RR	Reactor Refilling
ROSA	Rig Of Safety Assessment program
RPV	Reactor Pressure Vessel
SCRAM	Safety Control Rod Axe Man
SG	Steam Generator
TMI	Three Miles Island accident
VRC	Volume Rate of Change

v Related to vapour phase *w* Related to walls *Superscripts* ′ Partial derivative + Dimensionless variable – Averaged value · Variation over time	

2. Description of the facilities and the PWR

The BETHSY (Boucle d'Etude ThermoHydraulique SYstème) facility was defined by the French partners Framatome, EDF and CEA (Equipe BETHSY, 1990). It was designed to simulate a Framatome three loops PWR with a full power of 2775 MWt – 900 MWe. BETHSY has three loops, three steam generators and one pressurizer. The facility was designed using the same scaling factor for power and volume, a full height scaling and a 1/100 scaled volume at full-pressure reference condition. The core is composed of 428 full-length electrically heated rods. The maximal core power is equal to 10% of the 1/100 nominal power of the reference reactor. i.e. 2.86 MWt. Each steam generator is composed of a tube bundle consisting of 34 full-size U-tubes. For the 6.2-TC test, the break unit is located on the side of the horizontal cold leg of the pressurizer loop.

The LSTF (Large Scale Test Facility) facility was defined by the Japan Atomic Energy Research Institute (JAERI) (The ROSA-V Group, 1985). It was designed to simulate a Westinghouse four loops PWR with a full power of 3423 MWt – 1100 MWe. LSTF has two loops, two steam generators and one pressurizer. The facility was also designed using a power-to-volume scaling factor, a full-height scaling and a 1/48 scaled volume at full-pressure reference condition. The core is composed of 1008 full-length electrically heated rods. The maximum core power is equal to 14% of the 1/48 nominal power of the reference reactor i.e. 10 MWt. Each steam generator is composed of a tube bundle consisting of 141 full-size U-tubes. The flow area is 1/48 scaled in the pressure vessel and 1/24 scaled in the cold and hot legs and in the steam generators. For the SB-CL-21 test, the break unit is located on the side of the horizontal cold leg of the loop without the pressurizer.

This work will use the simulation of the BETHSY 6.2-TC and LSTF SB-CL-21 tests using the CATHARE system code. Both input decks represent the primary and secondary systems. The primary side contains the Reactor Pressure Vessel (RPV), hot and cold legs (HL & CL) with main coolant pumps, the pressurizer and the U-tubes of the steam generators (SG). The systems also include Accumulator Injection Systems (AIS).

The Framatome three loops PWR reference reactor of BETHSY has been modelled using CATHARE. The core for a typical 900 MWe PWR consists of 157 fuel assemblies, each composed of 264 fuel rods, supplying the 2775 MWt.

The nodalization of the primary systems of BETHSY, LSTF and the PWR are shown in Figure 1. The RPV is divided into several sub-components: the core, the downcomer, the lower and upper plenums, the upper head, the upper head bypass and the guide tubes volume. Note that BETHSY has a core bypass.

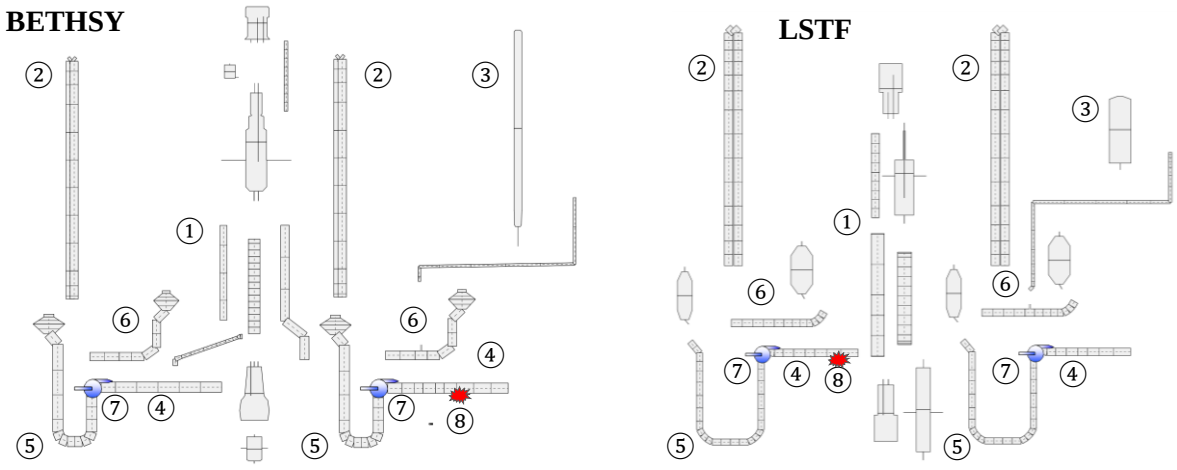

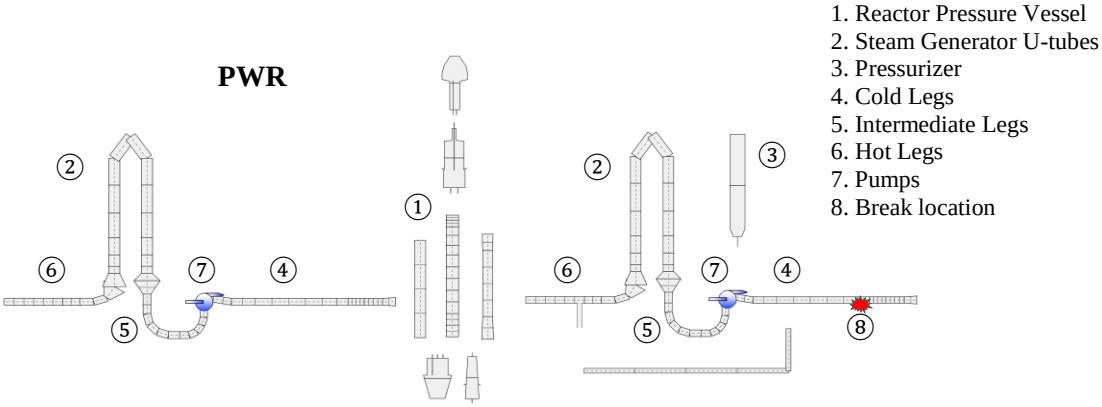

Figure 1. BETHSY, LSTF and PWR CATHARE nodalization of the primary system

As mentioned in the introduction, the current work aims to revisit the counterpart test between the 6.2-TC and the SB-CL-21 transients of the respective BETHSY and LSTF ITFs (D'Auria et al., 1992; Kumamaru et al., 1992). The main conditions of both tests were jointly defined by CEA and JAERI, with the main objectives being:

- To investigate design and scale effects between the two facilities for a SB-LOCA transient.
- To provide a data base for code assessment to better validate the extrapolation of this type of transient to nuclear plant.

This is why the 6% SB-LOCA code simulation of reference PWR of BETHSY is included in the initial counterpart test. However, it should then be highlighted that the LSTF reference reactor is different than the BETHSY reference reactor. As a result, LSTF may have inherent scaling differences with the simulated PWR due to the as well as the initial and boundary conditions. Therefore, some results related to the design differences of LSTF from BETHSY and the PWR are discussed in the analyses. The main characteristics of BETHSY, LSTF and the PWR are summarized in Table 1.

Table 1. Main characteristics of BETHSY, LSTF and the PWR

	BETHSY	LSTF	PWR
Reference reactor	F-PWR-3L	W-PWR-4L	-
Number of loops	3	2	3
Reference reactor loops number	3	4	-
Scaled volume	1/100	1/48	1/1
Scaled height	1/1	1/1	1/1
Scaled power	10 %	14 %	100 %
Maximum power	2.86 MWt	10.0 MWt	2775 MWt
Reference reactor maximum power	2775 MWt	3423 MWt	-
Total heated rods	428	1008	41448
Break area	$1.882 \cdot 10^{-4}$ m^2	$5.187 \cdot 10^{-4}$ m^2	$1.824 \cdot 10^{-2}$ m^2

3. The SB-LOCA transient

3.1. Description of the transient

The BETHSY 6.2-TC and LSTF SB-CL-21 tests scenarios consist of a cold leg SB-LOCA experiment without High Pressure Injection System (HPIS) and Auxiliary Feedwater (AFW) System. The ratios of break area, initial mass inventory and core power of LSTF to BETHSY are set to 2.76. This scaling factor is equal to the ratio of the SG U-tubes flow area, that is important to the liquid holdup phenomena in the SG U-tubes. The ratios of break area, initial mass inventory and core power of LSTF to BETHSY are set to 2.76. In both facilities, the break is equivalent to a 6 inches cold leg break, oriented horizontally, in their reference reactors. This break size corresponds to about respectively 5% and 6.5%

of the corresponding cold leg flow area in BETHSY and LSTF references reactors (Kumamaru et al., 1992).

The transient starts at operating full-pressure of 15.5 MPa and at 10% of the nominal scaled power. The reactor SCRAM signal occurs at 13 MPa resulting in the core power decay and pumps trip. The SG vapour lines are isolated and the set point of atmospheric relief valves is fixed to 7.2 MPa. The normal feedwater is stopped. The Accumulator Injection System (AIS) is activated at 4.2 MPa.

At the break opening, the primary fluid is mostly in subcooled liquid state. With decreasing pressure and decreasing mass inventory, the steam quality of discharged fluid at the break gradually increases. Throughout the transient, the main concern is the core cooling which may be challenged when a partially uncovered core induces a dry-out and a clad temperature excursion. This event mainly depends on the primary mass inventory, which itself strongly depends on the primary pressure evolution that influences the break flow rate and the safety injections. These two parameters are thus essential to describe the SB-LOCA transient.

The transient is divided into five chronological phases. These phases, also called "phenomenological windows", are characterized by phenomena and system parameters evolution. Bifurcating events that correspond to abrupt changes of phenomena, may occur during a phase or may delimit the phases. In the literature, usually 3, 4 or 5 phase splits, characterized by physical processes and phenomena, are defined for SB-LOCA transients. In the current study, the SB-LOCA is divided into 5 phases, inspired by the division made by the Polytechnic University of Valencia (Muñoz-Cobo et al., 2018), but adapted to a CL break. This choice allows separation of the dominant processes throughout the transient. The bifurcating events are summarized in Table 2.

Table 2. SB-LOCA phases and bifurcating events

Phases	Bifurcating events
1. Subcooled Blowdown (SBD)	A. Break opening
2. Natural Circulation (NC)	B. Pressurizer emptied, pump stop
3. Reflux Condenser Mode (RCM)	C. Top of SG tubes emptied (no liquid flow)
4. High-Quality Mixture Discharge (HQMD)	D. Primary-secondary pressure reversal
5. Reactor Refilling (RR)	E. Accumulator discharge

1. The Subcooled Blowdown phase:
After the opening of the break, the primary system depressurizes quickly from 15.5 MPa to about 8.0 MPa. The SCRAM signal triggers at around 6 seconds. For the facilities, the reduced initial core power is maintained during 53 seconds after the SCRAM signal. Then, the core power will join the JAERI conservative decay power curve. For the PWR, the core power decreases because of the control rod insertion, following the decay power. The primary pump trip occurs at the SCRAM signal and pump speed decreases and stops in both facilities. For the PWR, the pumps rotation speed decreases more slowly due to a higher initial velocity, initiating the transition to the natural circulation. Flashing occurs almost instantly after the break opening in the hottest parts of the primary system. The end of the subcooled blowdown is defined as the emptying of the pressurizer (less than 1% of the initial liquid mass).

2. The Natural Circulation phase:
The pumps being stopped, the fluid circulation is due to the differences in density between the ascending and descending parts of the cooling loops. The ascending part is the core, the upper plenum, the HL and the ascending part of the SG U-tubes. The descending part is the descending part of the SG U-tubes, the CL, and the vessel downcomer. Friction and singular pressure losses compensate for the difference in gravity in the ascending and descending parts of the circuit. During this phase, the primary pressure decreases slowly and stays above the secondary pressure to be able to transfer energy to the SG. During this phase, the core provides more energy to the fluid than is lost at the break and the primary fluid

needs to give the rest of power to the SG. This requires a higher temperature and higher pressure than in the secondary side of the SG.

3. The Reflux Condenser Mode phase:
Some vapour created in the core condenses in the SG U-tubes. The condensate water is first entrained in co-current flow to the intermediate leg (IL) and the CL. Then the mass of water decreasing, the void fraction increases in SG tubes and the vapour is no more capable to entrain the condensate water to the top of the SG tubes. This is the end of the natural circulation (NC) and the beginning of the Reflux Condenser Mode (RCM). Some decay power is still removed by condensation in the SG. The condensate water flows back to the HL in the ascending part of SG tubes whereas the condensate in the descending part of SG tubes fills the IL (Loop Seal Plugging (LSP)). With the stop of NC, water tends to settle in the lower part of the circuit, the steam quality at the break increases and more power is evacuated at the break. The plugs created in the IL isolate the CL and HL resulting in a faster pressure decrease in the CL due to the break. The remaining liquid mass in the IL is not available to cool the core and creates an unfavourable pressure difference, which induces a core uncovery. This core uncovery creates a dry-out and a temperature excursion with a first Peak Clad Temperature (PCT). The Loop Seal Clearing (LSC) phenomenon occurs when there is a sufficient pressure difference between the HL and CL to evacuate the plugs towards the pressure vessel. This ends the core uncovery and temperature excursion.

4. The High-Quality Mixture Discharge phase:
The beginning of this phase is marked by the passage of the primary pressure below the secondary pressure. From this moment, the heat flux at the SG U-tubes is reversed. During this phase, the pressure decreases significantly. The liquid level in CL goes down until it reaches the height of the break. The discharge at the break is then almost pure vapour, accelerating the depressurization.

5. The Reactor Refilling phase:
This phase starts when the accumulator injection is triggered. A large flow rate of sub-cooled liquid is discharged into the primary system thanks to AIS. From the beginning to the end of the accumulator discharge, the pressure decreases and the mass inventory starts increasing.

3.2. Experimental and simulated results: comparison between facilities and PWR

The phenomenological analysis of the BETHSY 6.2-TC, LSTF SB-CL-21 and PWR tests is presented in this section. When available, CATHARE predictions and experimental results are displayed together. The parameter evolutions are shown as normalized values, which are the values at any given time divided by a representative value (e.g. initial or maximum value). Table 3 provides a comparison of initial and boundary conditions at steady state, between experimental measured data and code predictions.

Table 3. Steady state comparison of initial and boundary conditions of the 6% SB-LOCA counterpart test between experimental data and code predictions

	BETHSY 6.2-TC		LSTF SB-CL-21		PWR
	EXP.	CATHARE	EXP.	CATHARE	CATHARE
Core power	2.86 MWt	2.84 MWt	7.93 MWt	7.93 MWt	2830 MWt
Primary system pressure	15.35 MPa	15.13 MPa	15.37 MPa	15.40 MPa	15.68 MPa
Secondary system pressure	6.85 MPa*	6.86 MPa*	7.00 MPa*	7.00 MPa*	5.78 MPa*
Pressurizer liquid level	7.45 m	7.35 m	1.70 m	1.70 m	7.32 m
Cold leg fluid temperature	285 °C*	285.2 °C*	287 °C*	287.2 °C*	280.0 °C*
Hot leg fluid temperature	316 °C*	316.1 °C*	317 °C*	316.6 °C*	315.7 °C*
Primary liquid mass	1984 kg	1947 kg	5404 kg	5543 kg	190 351 kg

*loops averaged

The initial test conditions predicted by CATHARE are found to be consistent with the experimental data. Minor differences that can be attributed to measurement uncertainties. For example, BETHSY experimental data are given with a core power uncertainty of 0.03 MWt, a pressure uncertainty of 0.15 MPa, a pressurizer liquid level uncertainty of 0.2 m and a primary liquid mass uncertainty of 50 kg.

In comparison to the PWR, the scaling of the two facilities respects the timing of events. Nonetheless, there are some minor differences between the experimental results and the CATHARE predictions, as well as between the facilities and the extrapolated PWR. Table 4 summarizes the main events that occurred during the transient. As examples of notable temporal differences or occurrences, consider the following:

- For this counterpart test, the pump coastdown of the facilities was not simulated to minimize the effect of different pump characteristics for the BETHSY and LSTF reference PWR (Kumamaru et al., 1992). Then, the time at which the pumps are stopped differs. Although the LSTF pumps take longer to stop than the BETHSY pumps, the main difference is the inertia of the PWR pumps, which prevents them from completely stopping.
- CATHARE predicts a too late pressurizer emptying.
- RCM phase events occur in the PWR later than in the facilities, resulting in a later primary-secondary pressure reversal.
- A second core uncovery leads to a second PCT on BETHSY, but not on LSTF nor on the PWR.
- Although the accumulator discharge occurs at roughly the same time, the discharge durations are vastly different.

Table 4. Chronology of the main events of the SB-LOCA transient

Event	BETHSY 6.2-TC		LSTF SB-CL-21		PWR
	EXP.	CATHARE	EXP.	CATHARE	CATHARE
1. SBD					
Break opening	0 s	0 s	0 s	0 s	0 s
SCRAM signal	8 s	6 s	6 s	6 s	5 s
Pump stopped	8 s	8 s	n/a	17 s	n/a
2. NC					
Pressurizer empty	18 s	24 s	16 s	30 s	15 s
3. RCM					
No flow rate at the top of SG tubes	~ 110 s	105 s	~ 110 s	101 s	153 s
First core uncovery	134 s	126 s	94 s	118 s	188 s
First Peak Clad Temperature	134 s	134 s	94 s	118 s	209 s
Loop Seal Plugging	140s	134 s	110 s	125 s	128 - 131 s
Loop Seal Clearing		151 s		154 s	161 - 146 s
4. HQMD					
Primary-secondary pressure reversal	176 s	175 s	165 s	160 s	229 s
Second core uncovery	342 s	355 s	n/a	n/a	n/a
Second Peak Clad Temperature	375 s	360 s	n/a	n/a	n/a
5. RR					
Activation of accumulator discharge	345 s	351 s	346 s	336 s	369 s
Minimum primary side mass	350 s	355 s	350 s	365 s	369 s
End of accumulator discharge	976 s	890 s	688 s	720 s	1467 s

n/a: not available

With the purpose to show some of the major evolutions, Figure 2 depicts the mass flow rate at the break. A rather good agreement between the code predictions and the experimental results is observed although the strange oscillatory results of LSTF (a possible measurement artefact) is not predicted by CATHARE. During the RCM phase, differences between BETHSY and LSTF are observed. In LSTF, the transition to high quality flow and then to vapour flow rate at the break occurs earlier than in BETHSY. This may be related to the geometry of two facilities: the volume above the break elevation is about 65% of the total primary volume in LSTF whereas it is 70% in BETHSY. This reflects

differences in the geometry of the reference reactors of the two facilities. The break flow rate predicted in the PWR simulation is lower than in the experiments up to the decrease due to high quality. It may be due to a longer pumps rotation, which brings a little higher quality at the break. As a result, the transition to high quality break flow is later than in the experiments as shown by the primary mass inventory in Figure 3.

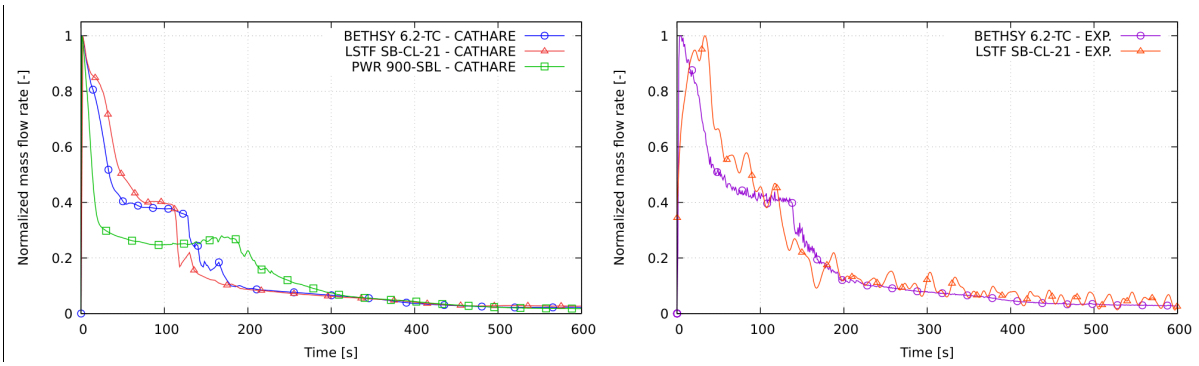

Figure 2. Break mass flow rate – predicted by CATHARE (left), experimental results (right)

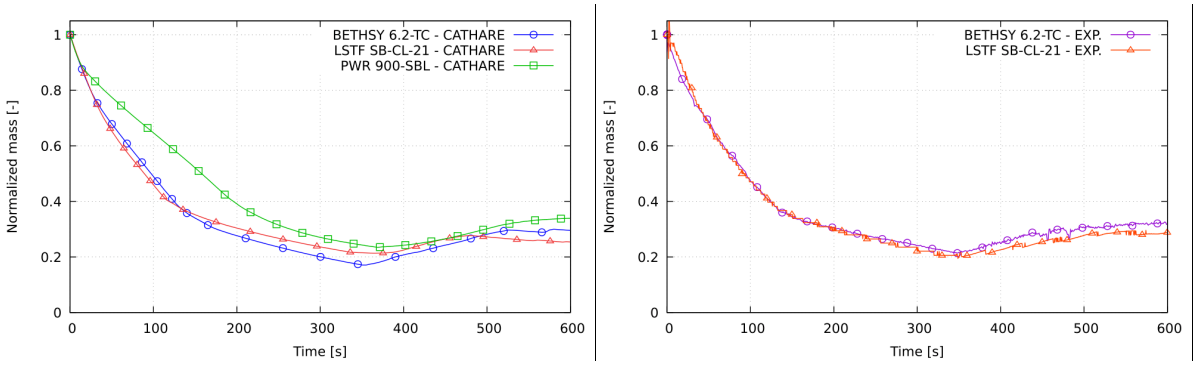

Figure 3. Primary mass inventory – predicted by CATHARE (left), experimental results (right)

Figure 4 depicts the primary system pressure. The pressure drops rapidly during the first seconds of the transient due to the liquid lost at the break and the pressurizer emptying. Then the pressure has a plateau above the secondary pressure as long as the core gives a higher power than the power lost at the break. This requires that the power difference is transferred to the secondary circuit. Finally, when there is a high quality flow at the break, the power lost at the break is higher than the core power and the system depressurizes below secondary pressure. As shown in Figure 4 (left) and Figure 4 (right), simulations provide pressure evolutions that are very close to the experimental values. There are some discrepancies between the facility results and the PWR predictions. During the SBD phase, the PWR primary system depressurizes more quickly and during the pressure plateau the PWR primary pressure is lower than in the experiment. It is worth mentioning that the BETHSY secondary pressure had to be increased to 6.85 MPa for the comparative test with LSTF, which differs from its PWR reference nominal pressure (5.78 MPa). This explains the pressure plateau difference between BETHSY and the PWR.

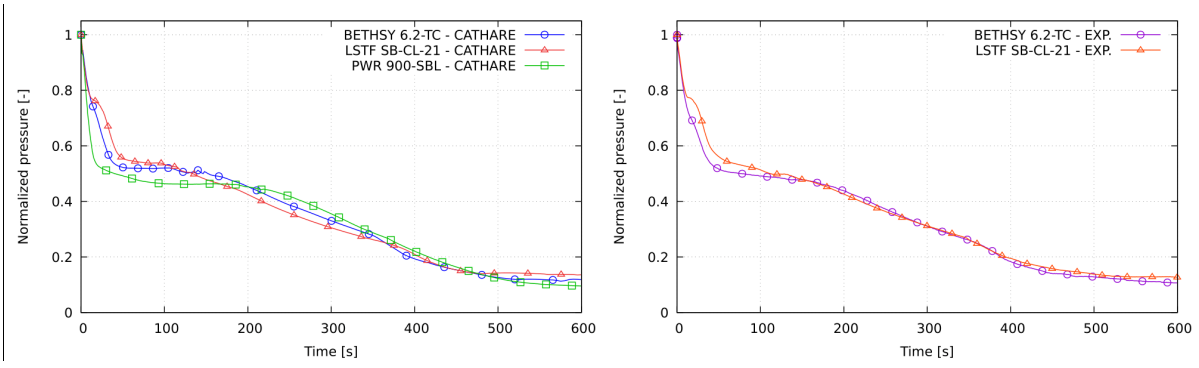

Figure 4. Primary pressure – predicted by CATHARE (left), experimental results (right)

For the 6% SB-LOCA tests, the initial core power is respectively 10% and 11% of nominal power of their reference reactors in BETHSY and LSTF although it is 100% in the reactor. After the SCRAM signal, the JAERI conservative power decay curve was used experimentally for BETHSY as well as for LSTF. However, the time at which the core power in the experiment leaves the scaled power was delayed to compensate the total core power delivered between 100% and the scaled power. Figure 5 shows the normalized power decay (power/initial power of the reference reactor). It is clear that the PWR power drop is faster than in the facilities. The three power curves evolve in a similar way only after about 300 seconds of transient.

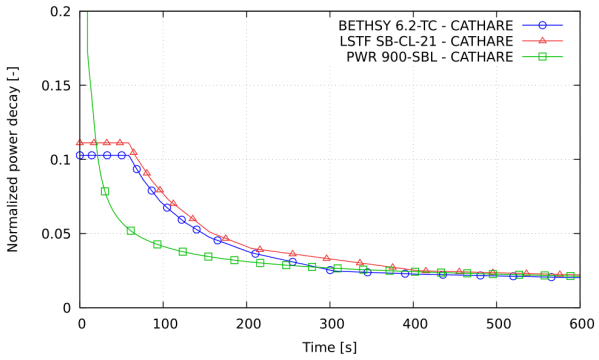

Figure 5. Core power decay – predicted by CATHARE

The core-collapsed level is an important parameter to consider, as it is directly related to the PCT safety criterion. Figure 6 and Figure 7 shows differences in the core collapsed level and the PCT. It is worth mentioning that the bottom elevation for the three cores is 0 m by definition (corresponding to 0 on the normalized collapsed level), and the top elevation (i.e. the height of the active rods) is 3.656 m for BETHSY and the French PWR and 3.660 m for LSTF (corresponding to 1 on the normalized collapsed level). On LSTF, the first core uncovery is almost total and occurs slightly earlier than on BETHSY. On BETHSY, there is a slight difference in the minimum collapsed level intensity between the code predictions and the experimental results. The PCT appears to be very sensitive to the duration of the core uncovery. Some differences between the code predictions and the experimental results are observed. The PWR core uncovery is predicted later than in BETHSY and LSTF (see Table 4). It should be noted that the PCT occurs at different elevations depending on the depth of the uncovering and on some reverse flow from upper plenum. The code predicts the PCT at 51% of the core height in BETHSY, 16% in LSTF and 75% in the PWR. The collapsed level remains at about 50 to 60% of the height after the loop seal clearing, which is sufficient to rewet the whole core height. Looking at the core power, it is higher in the PWR transient than in BETHSY and LSTF up to 22s and then it is higher from time 22s to about 300s. The distortions up to time 22s has less impact on core behaviour than the distortion between time 22s and 300s. Another choice could have been done with the experimental core power being equal to reactor power (divided by power ratio) as soon as core power reaches 10% of the nuclear power.

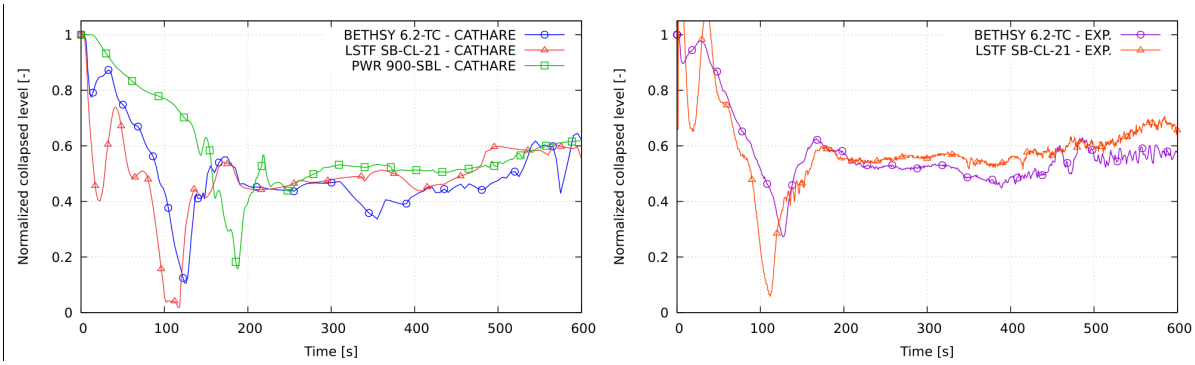

Figure 6. Core-collapsed level – predicted by CATHARE (left), experimental results (right)

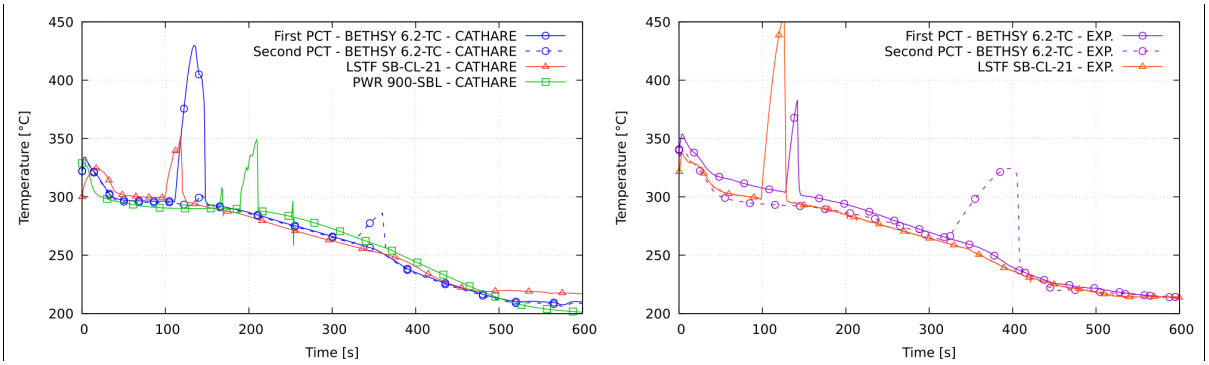

Figure 7. Peak Clad Temperature – predicted by CATHARE (left), experimental results (right)

4. Top-down scaling with FSA method

The FSA methodology (Zuber et al., 2007) is applied independently to each of the five transient phases. The Figure of Merit (FoM) for the SB-LOCA transient is defined as the Peak Clad Temperature (PCT) (Bestion et al., 2017; Zuber et al., 2007). The mass inventory M and the primary pressure P_1 are the two most important Parameters of Interest (PoI) that influence the FoM. Then, the equations for the evolution of primary mass and primary pressure are written. The pressurizer controls the primary pressure until it is empty, and then the mass and energy exchanges in the whole primary circuit control the primary pressure.

4.1. Mass balance equations in a volume V

The mass balance equation in a constant volume V is given by:

$$\frac{dM}{dt} \triangleq \dot{M} = \dot{M}_{in} - \dot{M}_{out} \tag{1}$$

$\dot{M}$ is the time rate change of fluid mass in V. $\dot{M}_{in}$ and $\dot{M}_{out}$ are respectively the mass flow rates entering and leaving V through fluid boundaries A_f. For a two-phase case, this equation can be split into liquid and vapour contributions. Mass balance equation becomes:

$$\dot{M} = \dot{M}_l + \dot{M}_v = \dot{M}_{l,in} - \dot{M}_{l,out} + \dot{M}_{v,in} - \dot{M}_{v,out} \tag{2}$$

The Eq. (2) applied to the primary system gives Eq. (3):

$$\dot{M}_1 = \dot{M}_{l,acc.} - \dot{M}_{l,break} - \dot{M}_{v,break} \tag{3}$$

Each contributor to the mass rate of change $\dot{M}$ is normalized with a time-average of the variables $\bar{Y}$ during the phases. Although the FSA method recommends normalization with an initial value Y_0 (Zuber et al., 2007), it is chosen here to use these average calculated values by a code.

$$Y^+(t) = \frac{Y(t)}{\bar{Y}} \tag{4}$$

The Eq. (3) then writes, introducing the Fractional Rate of Change (FRC) $\omega_{\dot{M},j}$, expressed in s^{-1} and quantifying the relative magnitude of the processes on the primary system mass (Wulff et al., 2009; Zuber et al., 2007):

$$\left.\frac{dM^+}{dt}\right|_1 = \omega_{\dot{M}_{l,acc.}} \cdot \dot{M}^+_{l,acc.} - \omega_{\dot{M}_{l,break}} \cdot \dot{M}^+_{l,break} - \omega_{\dot{M}_{v,break}} \cdot \dot{M}^+_{v,break} \tag{5}$$

The normalized mass balance equation is obtained, function of the *j* non-dimensional Agents of Change $\phi^+_{\dot{M},j}$ which define the processes acting on the mass rate of change $\dot{M}$:

$$\left.\frac{dM^+}{dt}\right|_1 = \omega_{\dot{M}_{l,acc.}} \cdot \phi^+_{\dot{M}_{l,acc.}} - \omega_{\dot{M}_{l,break}} \cdot \phi^+_{\dot{M}_{l,break}} - \omega_{\dot{M}_{v,break}} \cdot \phi^+_{\dot{M}_{v,break}} \tag{6}$$

4.2. Pressure equations in a volume V

The first principle of thermodynamics in a constant volume *V* with constant boundaries *A* to derive a total energy equation is written:

$$\frac{d}{dt}\int_V \rho\left(e+\frac{u^2}{2}\right)dV = \int_V \rho\left(\vec{F}\cdot\vec{u}+q_{ext}\right)dV - \int_{A_f} \rho\left(e+\frac{u^2}{2}\right)\vec{u}\cdot\vec{n}\,dA - \int_A \vec{q}\cdot\vec{n}\,dA - \int_{A_f}\left(\bar{\bar{T}}\cdot\vec{u}\right)\cdot\vec{n}\,dA \tag{7}$$

Some simplifications are considered by neglecting:
- The kinetic energy, which is much lower than the internal energy at low Mach numbers.
- The conductive heat flux along fluid boundaries, which is negligible compared to conductive heat flux along solid boundaries.
- External energy sources (radiative heat flux) q_{ext} and work of external force (gravity) $\left(\vec{F}\cdot\vec{u}\right)$, which is negligible compared to convective and diffusive energy fluxes when pumps are off.

Finally, the energy balance is expressed using enthalpy *h* instead of internal energy $\left(h=e+\frac{p}{\rho}\right)$. The two-phase energy balance equation for a volume *V* writes:

$$\frac{dM_l\cdot H_l}{dt} + \frac{dM_v\cdot H_v}{dt} - V\frac{dP}{dt} = W_w + \dot{M}_{l,in}\cdot h_{l,in} - \dot{M}_{l,out}\cdot H_l + \dot{M}_{v,in}\cdot h_{v,in} - \dot{M}_{v,out}\cdot H_v \tag{8}$$

With P, H_l and H_v representing the volume averaged pressure, specific liquid and vapour enthalpies, $h_{l,in}$ and $h_{v,in}$ representing the liquid and vapour entering specific enthalpies, and W_w representing the thermal power received from the walls. It is here assumed that the phases leave the volume with the mass weighted averaged specific enthalpy H_k of the volume.

Using the energy balance at the interfaces, the mass balance equation and a constant volume equation, a pressure equation expressed in terms of fluid volume rate of change is obtained (Bestion, 2020):

$$\begin{aligned}\left(\mu_l\cdot M_l + \mu_v\cdot M_v\right)\cdot\dot{P} &= \dot{M}_{l,in}\cdot\left[v_l + v'_{l,h}\cdot\left(h_{l,in} - H_l\right)\right] + \dot{M}_{v,in}\cdot\left[v_v + v'_{v,h}\cdot\left(h_{v,in} - H_v\right)\right] \\ &- \dot{M}_{l,out}\cdot v_l - \dot{M}_{v,out}\cdot v_v + v'_{l,h}\cdot W_{w,l} + v'_{v,h}\cdot W_{w,v} + v'_{l,h}\cdot W_{i,l} + v'_{v,h}\cdot W_{i,v} - \frac{W_{i,v}+W_{i,l}}{\varpi} + \frac{W_{w,i}}{\varpi}\end{aligned} \tag{9}$$

With:

$$v'_{k,p} \triangleq \left.\frac{\partial v_k}{\partial p}\right|_{h_k} \;;\; v'_{k,h} \triangleq \left.\frac{\partial v_k}{\partial h_k}\right|_p \;;\quad \mu_k = -v'_{k,p} - v_k\cdot v'_{k,h} \;;\; \varpi \triangleq \frac{H_v - H_l}{v_v - v_l}$$

Each term of the equation represents a volume rate of change of fluid (VRC, measured in m^3/s). The term on the l.h.s is the VRC corresponding to fluid expansion in depressurization. On the r.h.s, the terms are:
- The VRC due to entering liquid and vapour volume flow rates and the associated thermal expansion when mixing with internal fluid.

- The VRC by exiting liquid and vapour flow rates.
- The VRC by liquid and vapour thermal expansion by wall heating and by interfacial exchanges.
- The VRC by vaporization or condensation.
- The VRC by wall boiling or condensation.

This formulation provides an easy interpretation of the impact of fluid volume changes on pressure. Fluid volume may change by mass source or sink at boundaries, by heat exchange expansion/contraction, by vaporization or condensation and by isentropic expansion/contraction. The total volume being constant, when the r.h.s terms create volume, the pressure increases to lose the same volume by contraction (l.h.s term). When the r.h.s terms lose some volume, the depressurization compensates by fluid expansion (l.h.s term).

The Eq. (9) applied to the primary system gives Eq. (10):

$$\begin{aligned}\left(\mu_l \cdot M_l + \mu_v \cdot M_v\right) \cdot \dot{P}_1 = {} & \dot{M}_{l,acc.} \cdot v_l + \dot{M}_{l,acc.} \cdot v'_{l,h} \cdot \left(h_{l,acc.} - H_l\right) - \dot{M}_{l,break} \cdot v_l - \dot{M}_{v,break} \cdot v_v \\ & + v'_{l,h} \cdot W_{wl,core} + v'_{v,h} \cdot W_{wv,core} + \frac{W_{wi,core}}{\varpi} + v'_{l,h} \cdot W_{il,core} + v'_{v,h} \cdot W_{iv,core} - \frac{W_{iv,core} + W_{il,core}}{\varpi} \\ & + v'_{l,h} \cdot W_{wl,SG} + v'_{v,h} \cdot W_{wv,SG} + \frac{W_{wi,SG}}{\varpi} + v'_{l,h} \cdot W_{il,SG} + v'_{v,h} \cdot W_{iv,SG} - \frac{W_{iv,SG} + W_{il,SG}}{\varpi} \\ & + v'_{l,h} \cdot W_{owl} + v'_{v,h} \cdot W_{owv} + \frac{W_{owi}}{\varpi} + v'_{l,h} \cdot W_{il,ov} + v'_{v,h} \cdot W_{iv,ov} - \frac{W_{iv,ov} + W_{il,ov}}{\varpi}\end{aligned} \tag{10}$$

To simplify the pressure change due to VRC, the global expansion coefficient K is defined:

$$K = \left(\mu_l \cdot M_l + \mu_v \cdot M_v\right) \tag{11}$$

Each contributor to the pressure rate of change $\dot{P}$ is normalized in the same way as above (4). The Eq. (10) then writes, introducing the Fractional Rate of Change (FRC) $\omega_{\dot{P},j}$, expressed in s^{-1} and quantifying the relative magnitude of the processes on the primary system pressure (Wulff et al., 2009; Zuber et al., 2007):

$$\begin{aligned}\left.\frac{dP^+}{dt}\right|_1 = {} & \omega_{\dot{P},Q_{l,acc.}} \cdot \frac{\dot{M}^+_{l,acc.} \cdot v^+_l}{K^+} + \omega_{\dot{P},Q_{cond,l,acc.}} \cdot \frac{\dot{M}^+_{l,acc.} \cdot v'^+_{l,h} \cdot \left(h^+_{l,acc.} - H^+_l\right)}{K^+} \\ & - \omega_{\dot{P},Q_{l,break}} \cdot \frac{\dot{M}^+_{l,break} \cdot v^+_l}{K^+} - \omega_{\dot{P},Q_{v,break}} \cdot \frac{\dot{M}^+_{v,break} \cdot v^+_v}{K^+} \\ & + \omega_{\dot{P},Q_{wl,core}} \cdot \frac{v'^+_{l,h} \cdot W^+_{wl,core}}{K^+} + \omega_{\dot{P},Q_{wv,core}} \cdot \frac{v'^+_{v,h} \cdot W^+_{wv,core}}{K^+} + \omega_{\dot{P},Q_{wi,core}} \cdot \frac{W^+_{wi,core}}{K^+ \cdot \varpi^+} \\ & + \omega_{\dot{P},Q_{il,core}} \cdot \frac{v'^+_{l,h} \cdot W^+_{il,core}}{K^+} + \omega_{\dot{P},Q_{iv,core}} \cdot \frac{v'^+_{v,h} \cdot W^+_{iv,core}}{K^+} - \omega_{\dot{P},Q_{i,core}} \cdot \frac{W^+_{iv,core} + W^+_{il,core}}{K^+ \cdot \varpi^+} \\ & + \omega_{\dot{P},Q_{wl,SG}} \cdot \frac{v'^+_{l,h} \cdot W^+_{wl,SG}}{K^+} + \omega_{\dot{P},Q_{wv,SG}} \cdot \frac{v'^+_{v,h} \cdot W^+_{wv,SG}}{K^+} + \omega_{\dot{P},Q_{wi,SG}} \cdot \frac{W^+_{wi,SG}}{K^+ \cdot \varpi^+} \\ & + \omega_{\dot{P},Q_{il,SG}} \cdot \frac{v'^+_{l,h} \cdot W^+_{il,SG}}{K^+} + \omega_{\dot{P},Q_{iv,SG}} \cdot \frac{v'^+_{v,h} \cdot W^+_{iv,SG}}{K^+} - \omega_{\dot{P},Q_{i,SG}} \cdot \frac{W^+_{iv,SG} + W^+_{il,SG}}{K^+ \cdot \varpi^+} \\ & + \omega_{\dot{P},Q_{owl}} \cdot \frac{v'^+_{l,h} \cdot W^+_{owl}}{K^+} + \omega_{\dot{P},Q_{owv}} \cdot \frac{v'^+_{v,h} \cdot W^+_{owv}}{K^+} + \omega_{\dot{P},Q_{owi}} \cdot \frac{W^+_{owi}}{K^+ \cdot \varpi^+} \\ & + \omega_{\dot{P},Q_{il,ov}} \cdot \frac{v'^+_{l,h} \cdot W^+_{il,ov}}{K^+} + \omega_{\dot{P},Q_{iv,ov}} \cdot \frac{v'^+_{v,h} \cdot W^+_{iv,ov}}{K^+} - \omega_{\dot{P},Q_{i,ov}} \cdot \frac{W^+_{iv,ov} + W^+_{i,ov}}{K^+ \cdot \varpi^+}\end{aligned} \tag{12}$$

The normalized pressure equation is obtained, function of the j non-dimensional Agents of Change $\phi^+_{\dot{P},j}$ which define the processes acting on $\dot{P}$:

$$
\begin{aligned}
\left.\frac{dP^+}{dt}\right|_1 = {} & \omega_{\dot{P},Q_{l,acc.}} \cdot \phi^+_{\dot{P},Q_{l,acc.}} + \omega_{\dot{P},Q_{cond,l,acc..}} \cdot \phi^+_{\dot{P},Q_{cond,l,acc.}} \\
& - \omega_{\dot{P},Q_{l,break}} \cdot \phi^+_{\dot{P},Q_{l,break}} - \omega_{\dot{P},Q_{v,break}} \cdot \phi^+_{\dot{P},Q_{v,break}} \\
& + \omega_{\dot{P},Q_{wl,core}} \cdot \phi^+_{\dot{P},Q_{wl,core}} + \omega_{\dot{P},Q_{wv,core}} \cdot \phi^+_{\dot{P},Q_{wv,core}} + \omega_{\dot{P},Q_{wi,core}} \cdot \phi^+_{\dot{P},Q_{wi,core}} \\
& + \omega_{\dot{P},Q_{il,core}} \cdot \phi^+_{\dot{P},Q_{il,core}} + \omega_{\dot{P},Q_{iv,core}} \cdot \phi^+_{\dot{P},Q_{iv,core}} - \omega_{\dot{P},Q_{i,core}} \cdot \phi^+_{\dot{P},Q_{i,core}} \\
& + \omega_{\dot{P},Q_{wl,SG}} \cdot \phi^+_{\dot{P},Q_{wl,SG}} + \omega_{\dot{P},Q_{wv,SG}} \cdot \phi^+_{\dot{P},Q_{wv,SG}} + \omega_{\dot{P},Q_{wi,SG}} \cdot \phi^+_{\dot{P},Q_{wi,SG}} \\
& + \omega_{\dot{P},Q_{il,SG}} \cdot \phi^+_{\dot{P},Q_{il,SG}} + \omega_{\dot{P},Q_{iv,SG}} \cdot \phi^+_{\dot{P},Q_{iv,SG}} - \omega_{\dot{P},Q_{i,SG}} \cdot \phi^+_{\dot{P},Q_{i,SG}} \\
& + \omega_{\dot{P},Q_{owl}} \cdot \phi^+_{\dot{P},Q_{owl}} + \omega_{\dot{P},Q_{owv}} \cdot \phi^+_{\dot{P},Q_{owv}} + \omega_{\dot{P},Q_{owi}} \cdot \phi^+_{\dot{P},Q_{owi}} \\
& + \omega_{\dot{P},Q_{il,ov}} \cdot \phi^+_{\dot{P},Q_{il,ov}} + \omega_{\dot{P},Q_{iv,ov}} \cdot \phi^+_{\dot{P},Q_{iv,ov}} - \omega_{\dot{P},Q_{i,ov}} \cdot \phi^+_{\dot{P},Q_{i,ov}}
\end{aligned}
\tag{13}
$$

The time scaling for relative importance of agents (Zuber et al., 2007; Wulff et al., 2009) is performed using Eq. (6) and (13). The dominant one divides the FRC. The effect metrics obtained by dividing the FRCs by the largest FRC as in (14) allows to compare the contributions of each Agents of Change:

$$
\Omega_{\dot{M},\chi_j} = \frac{\omega_{\dot{M},\chi_j}}{\left|\omega_{\dot{M},\chi_D}\right|} \quad ; \quad \Omega_{\dot{P},\chi_j} = \frac{\omega_{\dot{P},\chi_j}}{\left|\omega_{\dot{P},\chi_D}\right|} \tag{14}
$$

4.3. Results of the a posteriori scaling analysis of the Subcooled Blowdown (SBD) phase

The volume of fluid lost at the break is replaced mainly by vaporization (flashing) and by fluid expansion. The water in the pressurizer is initially saturated and becomes superheated due to pressure decrease. In the rest of the primary circuit the water remains sub-cooled until it reaches saturation and starts flashing. The pressurizer is the key component at the start of the SBD phase since it controls the primary pressure. The emptying of the pressurizer is the bifurcating event that determines the end of this phase. Figure 8 shows the pressurizer emptying behaviour. Since the LSTF pressurizer is scaled with volume and has a reduced-height compared to the BETHSY and the PWR pressurizers, the emptying is normalized with the liquid volume instead of the liquid level.

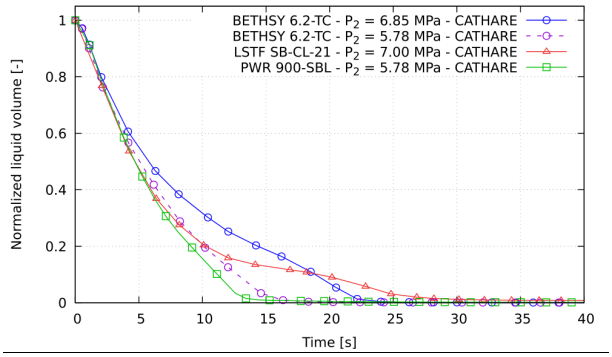

Figure 8. Pressurizer liquid volume during the SBD phase – predicted by CATHARE

The pressurizer emptying appears slightly different between the facilities and the PWR. The difference in the BETHSY pressurizer emptying compared to the PWR is due to the increase in the initial secondary pressure for the comparative test with LSTF in the counterpart test. The difference in the LSTF pressurizer emptying compared to BETHSY and the PWR would appears to be caused by its different geometry and its lower initial liquid level. This difference causes a distorted ratio between the pressurizer initial mass and the total mass of the primary system (see Table 5). It should be noted that the LSTF pressurizer design has been revised to simulate the pressurizer of the AP1000. It is relatively larger than the pressurizer of the conventional Westinghouse PWR (Cummins et al., 2003).

Table 5. Pressurizers design data

	BETHSY	LSTF	PWR
PRZ inner diameter	0.210 m	0.600 m	3.650 m
PRZ height	11.931 m	4.187 m	11.520 m
PRZ initial liquid level ratio	0.62	0.41	0.64
PRZ/primary initial liquid mass ratio	$8.43 \cdot 10^{-2}$	$6.38 \cdot 10^{-2}$	$8.68 \cdot 10^{-2}$

The depressurization of the SBD phase is also subject to distortions, as shown in Figure 9. As discussed in the section 3.1, the core power decay could explain the PWR higher depressurization as well as the initial secondary pressure (see the predicted primary pressure on BETHSY with the initial reference PWR secondary pressure of 5.78 MPa). The different connections to the pressurizer might explain the minor discrepancies amongst the BETHY and LSTF facilities (the pressurizer is connected to the intact loop in LSTF and to the broken loop in BETHSY).

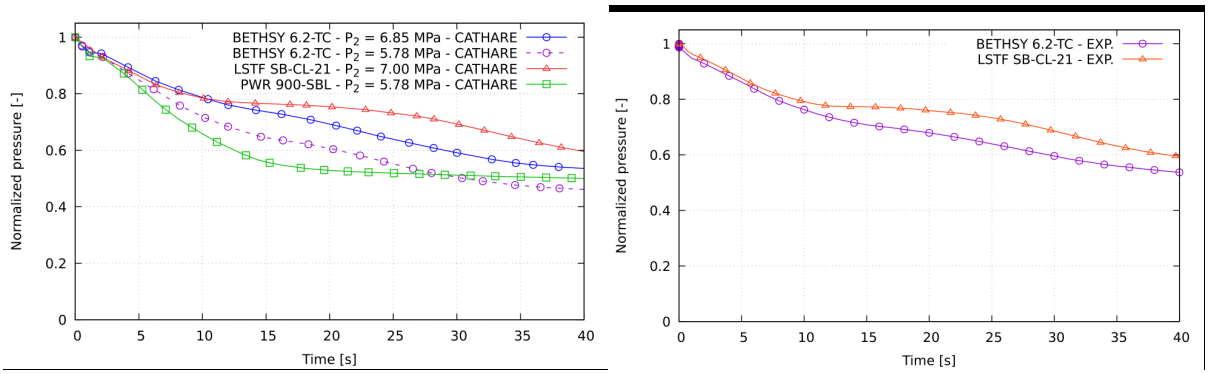

Figure 9. Primary pressure during the SBD phase – predicted by CATHARE (left), experimental results (right)

The depressurization of the SBD phase is investigated using the FSA method applied to mass and pressure (VRC) equations, for the primary system and the pressurizer control volumes. Table 6 shows the main parameters of the SBD phase.

Table 6. Main parameters of the SBD phase – predicted by CATHARE

	BETHSY	LSTF	PWR
Initial primary mass $M_{l,0}$	1 963 kg	5 612 kg	191 935 kg
Initial pressurizer liquid mass $M_{prz,l,0}$	150 kg	290 kg	15 077 kg
Phase duration Δt_{SBD}	24 s	30 s	15 s
Primary mass difference ΔM_l	384 kg	1 339 kg	22 607 kg
Pressurizer mass difference ΔM_{prz}	143 kg	285 kg	14 594 kg
Pressure difference ΔP_{SBD}	5.32 MPa	4.76 MPa	6.98 MPa
Averaged mass flow rate at the break $\overline{\dot{M}}_{break}$	15.20 kg/s	41.42 kg/s	1 321.5 kg/s
Averaged mass flow rate leaving the PRZ $\overline{\dot{M}}_{prz}$	6.24 kg/s	8.16 kg/s	819.89 kg/s
Averaged core power $\overline{W}_{core}$	$2.79 \cdot 10^6$ W	$8.13 \cdot 10^6$ W	$1.97 \cdot 10^9$ W
Averaged core power ratio (facilities/PWR)	1/706	1/242	-
Averaged SG tubes heat exchanges $\overline{W}_{SG}$	$3.93 \cdot 10^6$ W	$9.90 \cdot 10^6$ W	$2.11 \cdot 10^9$ W
Averaged primary wall heat exchanges $\overline{W}_{l,ow}$	$1.39 \cdot 10^5$ W	$1.51 \cdot 10^5$ W	$2.19 \cdot 10^7$ W
Averaged PRZ wall heat exchanges $\overline{W}_{prz,w}$	$2.20 \cdot 10^5$ W	$6.55 \cdot 10^4$ W	$1.24 \cdot 10^7$ W
Averaged liquid temperature $\overline{T}_{l,l}$	297.1 °C	298.2 °C	292.3 °C
Averaged vapour temperature $\overline{T}_{l,v}$	325.3 °C	325.4 °C	322.5 °C

As mentioned before, the pressurizer controls the primary pressure until its emptying. In addition to the scaling analysis on the primary system control volume, mass and pressure equations for the pressurizer

control volume are written for the SBD phase. These equations are obtained from the Eq. (2) and (9), giving respectively Eq. (15) and (16):

$$\dot{M}_{prz} = - \dot{M}_{l,prz} - \dot{M}_{v,prz} \tag{15}$$

$$\begin{aligned}\left(\mu_l \cdot M_l + \mu_v \cdot M_v\right) \cdot \dot{P}_{prz} &= - \dot{M}_{l,prz} \cdot v_l - \dot{M}_{v,prz} \cdot v_v \\ + v'_{l,h} \cdot W_{wl,prz} + v'_{v,h} \cdot W_{wv,prz} + \frac{W_{wi,prz}}{\varpi} &+ v'_{l,h} \cdot W_{il,prz} + v'_{v,h} \cdot W_{iv,prz} - \frac{W_{iv,prz}+W_{il,prz}}{\varpi}\end{aligned} \tag{16}$$

Giving the pressurizer mass and pressure FRC expressions, quantifying the relative magnitude of the processes on the pressurizer mass and pressure (Wulff et al., 2009; Zuber et al., 2007):

$$\left.\frac{dM^+}{dt}\right|_{prz} = - \omega_{\dot{M}_{l,prz}} \cdot \dot{M}^+_{l,prz} - \omega_{\dot{M}_{v,prz}} \cdot \dot{M}^+_{v,prz} \tag{17}$$

$$\begin{aligned}\left.\frac{dP^+}{dt}\right|_{prz} &= - \omega_{\dot{P},Q_{l,prz}} \cdot \frac{\dot{M}^+_{l,prz} \cdot v^+_l}{K^+} - \omega_{\dot{P},Q_{v,prz}} \cdot \frac{\dot{M}^+_{v,prz} \cdot v^+_v}{K^+} \\ + \omega_{\dot{P},Q_{wl,prz}} \cdot \frac{v'^+_{l,h} \cdot W^+_{wl,prz}}{K^+} &+ \omega_{\dot{P},Q_{wv,prz}} \cdot \frac{v'^+_{v,h} \cdot W^+_{wv,prz}}{K^+} + \omega_{\dot{P},Q_{wi,prz}} \cdot \frac{W^+_{wi,prz}}{K^+ \cdot \varpi^+} \\ + \omega_{\dot{P},Q_{il,prz}} \cdot \frac{v'^+_{l,h} \cdot W^+_{il,prz}}{K^+} &+ \omega_{\dot{P},Q_{iv,prz}} \cdot \frac{v'^+_{v,h} \cdot W^+_{iv,prz}}{K^+} - \omega_{\dot{P},Q_{i,prz}} \cdot \frac{W^+_{iv,prz}+W^+_{il,prz}}{K^+ \cdot \varpi^+}\end{aligned} \tag{18}$$

And defining the non-dimensional Agents of Change acting on $\dot{M}_{prz}$ and $\dot{P}_{prz}$:

$$\left.\frac{dM^+}{dt}\right|_{prz} = - \omega_{\dot{M}_{l,prz}} \cdot \phi^+_{\dot{M}_{l,prz}} - \omega_{\dot{M}_{v,prz}} \cdot \phi^+_{\dot{M}_{v,prz}} \tag{19}$$

$$\begin{aligned}\left.\frac{dP^+}{dt}\right|_{prz} &= - \omega_{\dot{P},Q_{l,prz}} \cdot \phi^+_{\dot{P},Q_{l,prz}} - \omega_{\dot{P},Q_{v,prz}} \cdot \phi^+_{\dot{P},Q_{v,prz}} \\ + \omega_{\dot{P},Q_{wl,prz}} \cdot \phi^+_{\dot{P},Q_{wl,prz}} &+ \omega_{\dot{P},Q_{wv,prz}} \cdot \phi^+_{\dot{P},Q_{wv,prz}} + \omega_{\dot{P},Q_{wi,prz}} \cdot \phi^+_{\dot{P},Q_{wi,prz}} \\ + \omega_{\dot{P},Q_{il,prz}} \cdot \phi^+_{\dot{P},Q_{il,prz}} &+ \omega_{\dot{P},Q_{iv,prz}} \cdot \phi^+_{\dot{P},Q_{iv,prz}} - \omega_{\dot{P},Q_{i,prz}} \cdot \phi^+_{\dot{P},Q_{i,prz}}\end{aligned} \tag{20}$$

The time scaling for relative importance of agents is applied to Eq. (19) and (20) in the same way it is applied in Eq. (14). Table 7 and Table 8 show the values of the effect metrics for the mass equation $\Omega_{\dot{M},j}$ and the pressure equation $\Omega_{\dot{P},j}$ for the SBD phase for the pressurizer and the primary system, respectively.

Table 7. Effect metrics of the pressurizer during the SBD phase

		BETHSY	LSTF	PWR
Rate of mass change due to the contribution by:				
Liquid flow rate leaving the pressurizer	$\Omega_{\dot{M}_{l,prz}}$	**-1.000**	**-1.000**	**-1.000**
Vapour flow rate leaving the pressurizer	$\Omega_{\dot{M}_{v,prz}}$	-0.002	-0.001	-0.004
Rate of pressure change due to the contribution by:				
Liquid volume flow rate leaving the pressurizer	$\Omega_{\dot{P},Q_{l,prz}}$	**-1.000**	**-1.000**	**-1.000**
Vapour volume flow rate leaving the pressurizer	$\Omega_{\dot{P},Q_{v,prz}}$	**-0.298**	**-0.269**	**-0.649**

Thermal expansion/contraction by wall-liquid heat transfers in the pressurizer	$\Omega_{\dot{P},Q_{wl,prz}}$	0.003	0.000	0.000
Thermal expansion/contraction by wall-vapour heat transfers in the pressurizer	$\Omega_{\dot{P},Q_{wv,prz}}$	0.013	0.000	0.000
Volume change by wall boiling or condensation in the pressurizer	$\Omega_{\dot{P},Q_{wi,prz}}$	**0.163**	0.029	**0.080**
Thermal expansion/contraction by interface-liquid heat transfers in the pressurizer	$\Omega_{\dot{P},Q_{il,prz}}$	**-0.062**	**-0.067**	**-0.102**
Thermal expansion/contraction by interface-vapour heat transfers in the pressurizer	$\Omega_{\dot{P},Q_{iv,prz}}$	**0.290**	**0.466**	**0.437**
Volume change by vaporization or condensation by interfacial transfers in the pressurizer	$\Omega_{\dot{P},Q_{i,prz}}$	**0.448**	**0.230**	**0.584**

The mass and pressure rate of change in the pressurizer are mainly due to the liquid flow rate leaving the pressurizer. The vapour mass flow rate leaving the pressurizer is negligible in the CATHARE code calculation. Nevertheless, the vapour volume flow rate contributes significantly to pressure decrease, as demonstrated by the effect metrics contributing to the pressure change. It should be noted that the predicted impact of the vapour volume flow rate is lower in the facilities (BETHSY: -0.298; LSTF: -0.269) than in the PWR (-0.649). Because the same ratio between the initial liquid mass of the pressurizer and the initial mass of the primary system is found, it can be deduced that the additional contribution of the predicted vapour exit flow rate for the PWR is related to the faster depressurization which creates more flashing of the water (see Table 5). Because of the sudden pressure decrease, the vaporization is an influent process in all three systems but it is found to be smaller in LSTF (0.230) than in BETHSY (0.448) and the PWR (0.584). The higher contribution of the predicted vapour exiting flow rate for the PWR is related to the faster depressurization which creates more flashing of the water (see Figure 9). One may add that a simple 2-node modelling of the pressurizer with CATHARE cannot predict the void fraction gradient from the bottom to the water level and then cannot predict very precisely the void fraction entrained in the expansion line. This suggests that a 1-D modelling of the pressurizer with smaller meshes could be more precise. Because the pressurizer height was preserved in BETHSY, the ratio of the walls exchange surface to volume is higher than in LSTF, where the height was reduced (see Table 5). Because the pressurizer heaters are turned off prior to the start of the transient, only the wall and interfacial heat exchange terms remain.

Table 8. Effect metrics of the primary system during the SBD phase

		BETHSY	LSTF	PWR
Rate of mass change due to the contribution by:				
Liquid flow rate leaving the primary system through the break	$\Omega_{\dot{M}_{l,break}}$	**-1.000**	**-1.000**	**-1.000**
Vapour flow rate leaving the primary system through the break	$\Omega_{\dot{M}_{v,break}}$	-0.013	-0.015	-0.019
Rate of pressure change due to the contribution by:				
Liquid volume flow rate leaving the primary system through the break	$\Omega_{\dot{P},Q_{l,break}}$	**-1.000**	**-1.000**	**-0.718**
Vapour volume flow rate leaving the primary system through the break	$\Omega_{\dot{P},Q_{v,break}}$	**-0.129**	**-0.153**	**-0.155**
Thermal expansion/contraction by wall-liquid heat transfers in the core	$\Omega_{\dot{P},Q_{wl,core}}$	**0.053**	0.022	**0.604**
Thermal expansion/contraction by wall-vapour heat transfers in the core	$\Omega_{\dot{P},Q_{wv,core}}$	0.000	0.004	0.000
Volume change by wall boiling or condensation in the core	$\Omega_{\dot{P},Q_{wi,core}}$	**0.593**	**0.668**	**0.075**
Thermal expansion/contraction by interface-liquid heat transfers in the core	$\Omega_{\dot{P},Q_{il,core}}$	0.010	0.008	0.002
Thermal expansion/contraction by interface-vapour heat transfers in the core	$\Omega_{\dot{P},Q_{iv,core}}$	0.005	0.007	0.000
Volume change by vaporization or condensation by interfacial transfers in the core	$\Omega_{\dot{P},Q_{i,core}}$	**-0.130**	**-0.101**	-0.030

Thermal expansion/contraction by wall-liquid heat transfers in SG tubes	$\Omega_{\dot{P},Q_{wl,SG}}$	**-0.138**	**-0.126**	**-1.000**
Thermal expansion/contraction by wall-vapour heat transfers in SG tubes	$\Omega_{\dot{P},Q_{wv,SG}}$	0.000	0.000	0.000
Volume change by wall boiling or condensation in SG tubes	$\Omega_{\dot{P},Q_{wi,SG}}$	0.000	0.000	0.000
Thermal expansion/contraction by interface-liquid heat transfers in the SG tubes	$\Omega_{\dot{P},Q_{il,SG}}$	0.036	0.033	0.031
Thermal expansion/contraction by interface-vapour heat transfers in the SG tubes	$\Omega_{\dot{P},Q_{iv,SG}}$	0.004	0.003	0.004
Volume change by vaporization or condensation by interfacial transfers in the SG tubes	$\Omega_{\dot{P},Q_{i,SG}}$	**-0.473**	**-0.425**	**-0.455**
Thermal expansion/contraction by wall-liquid heat transfers in the primary system*	$\Omega_{\dot{P},Q_{owl}}$	-0.006	0.000	-0.003
Thermal expansion/contraction by wall-vapour heat transfers in the primary system*	$\Omega_{\dot{P},Q_{owv}}$	0.005	0.000	0.000
Volume change by wall boiling or condensation in the primary system*	$\Omega_{\dot{P},Q_{owi}}$	0.031	0.018	**0.087**
Thermal expansion/contraction by interface-liquid heat transfers in the primary system*	$\Omega_{\dot{P},Q_{il,ov}}$	-0.042	-0.014	-0.038
Thermal expansion/contraction by interface-vapour heat transfers in the primary system*	$\Omega_{\dot{P},Q_{iv,ov}}$	**0.183**	**0.133**	**0.253**
Volume change by vaporization or condensation by interfacial transfers in the primary system*	$\Omega_{\dot{P},Q_{i,ov}}$	**0.448**	**0.116**	**0.417**

*(except SG tubes and fuel rods)

The effect metric related to the liquid mass flow rate at the break has the greatest influence on the rate of mass change in the primary system control volume. The vapour break flow is contributing only a very small amount. Although measured data cannot confirm this repartition, this evaluation is easily accepted because almost only liquid water flows in the loops and in the pressure vessel during SBD phase.

The term related to the liquid volume flow rate at the break is seen to be dominant on the rate of primary pressure change in the facilities. This term contributes to system depressurization. Likewise, the thermal contraction caused by condensation by interfacial transfers in the SG tubes is regarded as influent for both facilities (BETHSY: -0.473; LSTF: -0.425) and the PWR (-0.455). The dominant process contributing to the PWR depressurization is the contraction by wall-liquid heat transfers in SG tubes. This process has limited impact in the facilities (BETHSY: -0.138; LSTF: -0.126). This is also corresponding to a situation with more vapour in loops during SBD in the PWR compared to the facilities. The volume change by vaporization in the primary system is one of the terms contributing to the pressurization. There is a difference in the impact of this phenomenon in LSTF (0.116) compared to BETHSY (0.448) and the PWR (0.417). Similarly, the term related to thermal expansion by interface-vapour heat transfers in the primary system volume is influent, but it is higher in the PWR (BETHSY: 0.183; LSTF: 0.133; PWR: 0.253). The relative effect of the volume change caused by wall boiling in the core is significant in the facilities (BETHSY: 0.593; LSTF: 0.668) but negligible in the PWR (0.075). On the contrary, the relative effect of the thermal expansion caused by wall-liquid heat transfers in the core is more important in the PWR (0.604) than in facilities (BETHSY: 0.053; LSTF: 0.022). This difference is explained by the lower averaged liquid temperature predicted in the PWR core (297.2°C) compared to BETHSY (307.4 °C) and LSTF (321.1 °C). The power provided by the PWR core is mostly transferred to heat the liquid, while in the facilities, with a liquid temperature closer to the saturation temperature, the core power leads to boiling.

The discrepancies in the process hierarchy between the simulated experiments and the PWR can be explained by the core initial power. During the SBD phase, the PWR core injects more power into the primary system compared to the BETHSY and LSTF cores, as shown in Figure 5. The PWR SG tubes transfer then more power from the core to the secondary system.

4.4. Results of the a posteriori scaling analysis of the Natural Circulation (NC) phase

The NC phase entry conditions were initially chosen as the emptying of the pressurizer and the primary pumps trip. However, as shown in Figure 10, the inertia of the PWR pumps prevents them from completely stopping. Since the pump coastdown was not simulated on the facilities, their speed rapidly decreases to zero, while the PWR pumps rotation gradually decreases because of the inertia. The distortion caused by the initial core power between the PWR and the facilities is still present in this phase (see Figure 5).

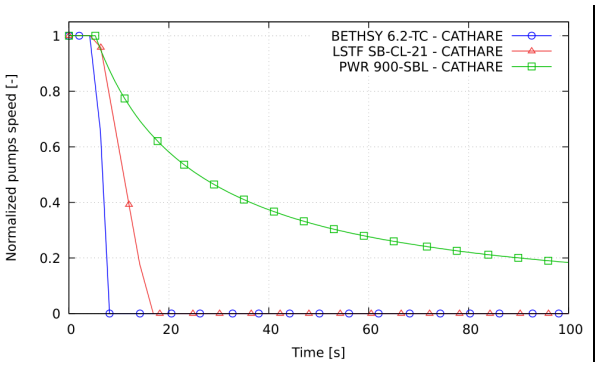

Figure 10. Primary pumps rotational speed – predicted by CATHARE

The NC phase continues until there is no more liquid mass flow rate at the top of the SG tubes. There is no longer any natural circulation in the primary circuit. Figure 11 demonstrates that the bifurcating event parameter does not evolve in the same way in all three systems. Although the flow rate at the top of the SG tubes decreases faster (after 38 seconds) on LSTF than on BETHSY, the occurrence of the zero flow rate occurs almost simultaneously. Because the pumps are still running at a reduced speed, the NC phase in the PWR lasts longer.

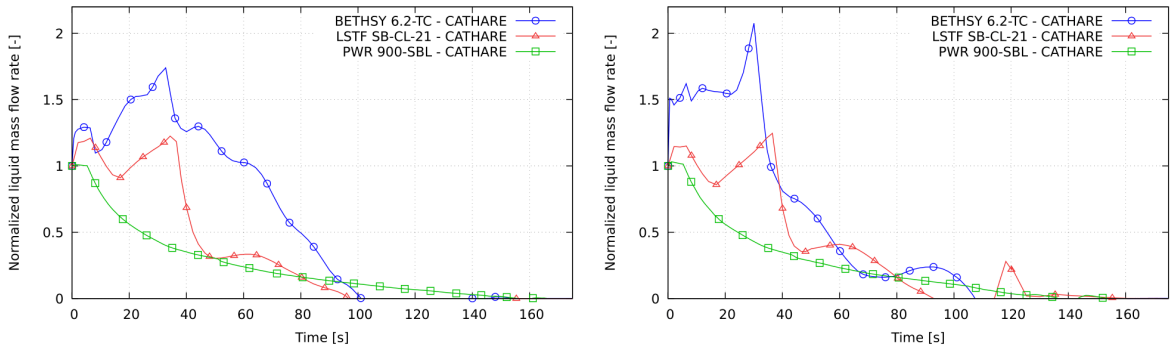

Figure 11. Liquid mass flow rate at the top of the SG tubes – intact loop(s) (left), broken loop (right) – predicted by CATHARE

The depressurization of the NC phase is investigated using the FSA method applied to mass and pressure (VRC) equations, for the primary system control volume. Table 9 shows the main parameters of the NC phase.

Table 9. Main parameters of the NC phase – predicted by CATHARE

	BETHSY	LSTF	PWR
Initial primary mass $M_{1,0}$	1 551 kg	4 198 kg	168 527 kg
Phase duration Δt_{NC}	81 s	70 s	138 s
Primary mass difference ΔM_1	623 kg	1 625 kg	69 637 kg
Pressure difference ΔP_{NC}	1.60 MPa	2.13 MPa	1.32 MPa
Averaged mass flow rate at the break $\bar{\dot{M}}_{break}$	8.03 kg/s	24.06 kg/s	526.59 kg/s
Averaged core power $\bar{W}_{core}$	$2.57 \cdot 10^6$ W	$7.37 \cdot 10^6$ W	$1.65 \cdot 10^8$ W

Averaged core power ratio (facilities/PWR)	1/64	1/22	-
Averaged SG tubes heat exchanges $\overline{W}_{SG}$	$2.23 \cdot 10^6$ W	$6.82 \cdot 10^6$ W	$1.39 \cdot 10^8$ W
Averaged primary wall heat exchanges $\overline{W}_{l,ow}$	$1.01 \cdot 10^5$ W	$1.47 \cdot 10^5$ W	$1.11 \cdot 10^7$ W
Averaged liquid temperature $\overline{T}_{l,l}$	292.0 °C	293.7 °C	289.1 °C
Averaged vapour temperature $\overline{T}_{l,v}$	298.3 °C	299.8 °C	290.7 °C

Table 10 displays the values of the effect metrics for the mass equation $\Omega_{\dot{M},j}$ and the pressure equation $\Omega_{\dot{P},j}$ for the primary system NC phase.

Table 10. Effect metrics of the primary system during the NC phase

		BETHSY	LSTF	PWR
Rate of mass change due to the contribution by:				
Liquid flow rate leaving the primary system through the break	$\Omega_{\dot{M}_{l,break}}$	**-1.000**	**-1.000**	**-1.000**
Vapour flow rate leaving the primary system through the break	$\Omega_{\dot{M}_{v,break}}$	**-0.087**	**-0.078**	**-0.171**
Rate of pressure change due to the contribution by:				
Liquid volume flow rate leaving the primary system through the break	$\Omega_{\dot{P},\dot{Q}_{l,break}}$	**-0.304**	**-0.358**	**-0.267**
Vapour volume flow rate leaving the primary system through the break	$\Omega_{\dot{P},\dot{Q}_{v,break}}$	**-0.463**	**-0.438**	**-0.846**
Thermal expansion/contraction by wall-liquid heat transfers in the core	$\Omega_{\dot{P},\dot{Q}_{wl,core}}$	0.009	0.007	0.012
Thermal expansion/contraction by wall-vapour heat transfers in the core	$\Omega_{\dot{P},\dot{Q}_{wv,core}}$	0.000	0.000	0.000
Volume change by wall boiling or condensation in the core	$\Omega_{\dot{P},\dot{Q}_{wi,core}}$	**1.000**	**0.736**	**1.000**
Thermal expansion/contraction by interface-liquid heat transfers in the core	$\Omega_{\dot{P},\dot{Q}_{il,core}}$	0.004	0.003	0.000
Thermal expansion/contraction by interface-vapour heat transfers in the core	$\Omega_{\dot{P},\dot{Q}_{iv,core}}$	0.001	0.003	0.000
Volume change by vaporization or condensation by interfacial transfers in the core	$\Omega_{\dot{P},\dot{Q}_{i,core}}$	**-0.087**	**-0.056**	0.001
Thermal expansion/contraction by wall-liquid heat transfers in SG tubes	$\Omega_{\dot{P},\dot{Q}_{wl,SG}}$	-0.048	**-0.058**	**-0.051**
Thermal expansion/contraction by wall-vapour heat transfers in SG tubes	$\Omega_{\dot{P},\dot{Q}_{wv,SG}}$	0.000	0.000	0.000
Volume change by wall boiling or condensation in SG tubes	$\Omega_{\dot{P},\dot{Q}_{wi,SG}}$	0.000	0.000	0.001
Thermal expansion/contraction by interface-liquid heat transfers in the SG tubes	$\Omega_{\dot{P},\dot{Q}_{il,SG}}$	0.041	**0.051**	0.032
Thermal expansion/contraction by interface-vapour heat transfers in the SG tubes	$\Omega_{\dot{P},\dot{Q}_{iv,SG}}$	0.005	0.013	0.003
Volume change by vaporization or condensation by interfacial transfers in the SG tubes	$\Omega_{\dot{P},\dot{Q}_{i,SG}}$	**-0.882**	**-1.000**	**-0.739**
Thermal expansion/contraction by wall-liquid heat transfers in the primary system*	$\Omega_{\dot{P},\dot{Q}_{owl}}$	-0.003	-0.001	-0.001
Thermal expansion/contraction by wall-vapour heat transfers in the primary system*	$\Omega_{\dot{P},\dot{Q}_{owv}}$	0.044	0.006	0.005
Volume change by wall boiling or condensation in the primary system*	$\Omega_{\dot{P},\dot{Q}_{owi}}$	**0.101**	0.043	**0.087**
Thermal expansion/contraction by interface-liquid heat transfers in the primary system*	$\Omega_{\dot{P},\dot{Q}_{il,ov}}$	-0.004	-0.007	-0.002
Thermal expansion/contraction by interface-vapour heat transfers in the primary system*	$\Omega_{\dot{P},\dot{Q}_{iv,ov}}$	0.006	0.046	0.011
Volume change by vaporization or condensation by interfacial transfers in the primary system*	$\Omega_{\dot{P},\dot{Q}_{i,ov}}$	**0.090**	**0.119**	0.044

*(except SG tubes and fuel rods)

The dominant effect metric on the rate of mass change remains the liquid mass flow rate at the break. Because of the boiling in the core, the vapour flow rate is slightly higher than in the SBD phase. Because of the higher relative power in the core, the PWR vapour mass flow rate is higher (-0.171) than in the facilities (BETHSY: -0.087; LSTF: -0.078). This difference could also possibly be due to the PWR pumps, which, unlike the facilities, are still operating and shift the natural convection.

The dominant effect metric on the pressurization is the volume change by wall-boiling in the core (BETHSY: 1.000; LSTF: 0.736; PWR: 1.000). This term is primarily balanced by volume change due to condensation by interfacial transfers in SG tubes (BETHSY: -0.882; LSTF: -1.000; PWR: -0.739) Note that the preponderant term is inverted on LSTF compared to BETHSY and PWR. The volume leaving the system at the break is also influent in the contribution to the depressurization. But the higher vapour generated in the PWR than in the facilities during the SBD phase is still visible during this NC phase (BETHSY: -0.463; LSTF: -0.438; PWR: -0.846). As shown in Figure 12, the ratio of vapour flow rate to liquid flow rate is distorted in the facilities compared to the PWR. Finally, the volume change due to wall-boiling in the primary system has little effect (BETHSY: 0.101; LSTF: 0.043; PWR: 0.087). However, because of its higher wall heat exchange surface to primary volume ratio, it is higher on BETHSY.

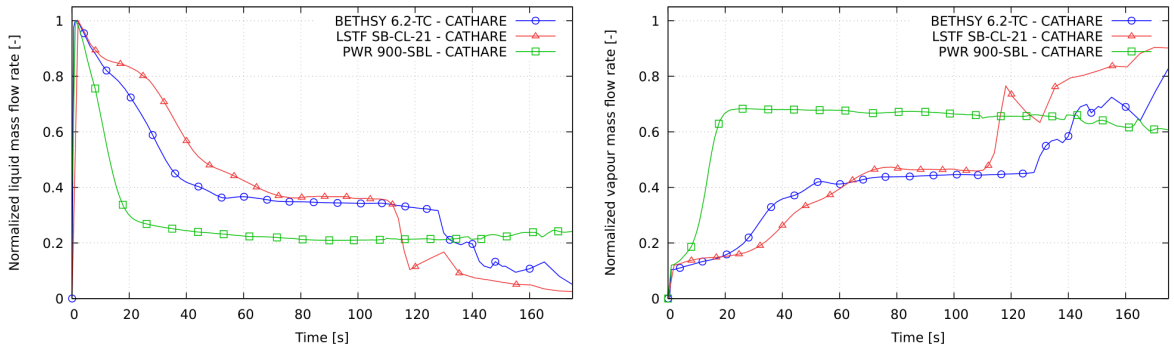

Figure 12. Break liquid (left) and vapour (right) mass flow rate – predicted by CATHARE

4.5. Results of the a posteriori scaling analysis of the Reflux Condenser Mode (RCM) phase

The primary system depressurization rate is nearly as low during the RCM phase as it is during the NC phase. Figure 13 depicts a transition of the void fraction in the CL upstream of the break. The break mass flow continues to transition from liquid to vapour, eventually reaching the HQMD phase. It can be seen that the facilities behaviour is distorted because of the premature stop of the pumps compared to the PWR.

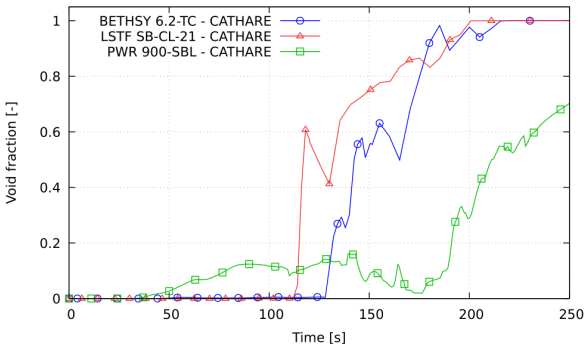

Figure 13. Void fraction in the CL upstream of the break – predicted by CATHARE

At end of NC, some liquid from SG tubes is accumulated in the intermediate legs and creates a plug which isolates the vapour of the region of the core, upper plenum, hot legs, inlet SG, header and upward half of SG tubes from the vapour of the region of the cold legs and downcomer. The pressure in the first region stabilizes above the secondary pressure while the pressure in the second region decreases due to

break flow. Figure 14 depicts the predicted Loop Seal Plugging (LSP) and Loop Seal Clearing (LSC) phenomena, which are responsible for core uncovery and core reflooding, respectively (see Figure 6). It is observed that CATHARE only predicts the LSP phenomenon on one IL of the facilities. This is predicted to occur only in the broken IL in BETHSY. On LSTF, however, it is predicted only in the intact IL.

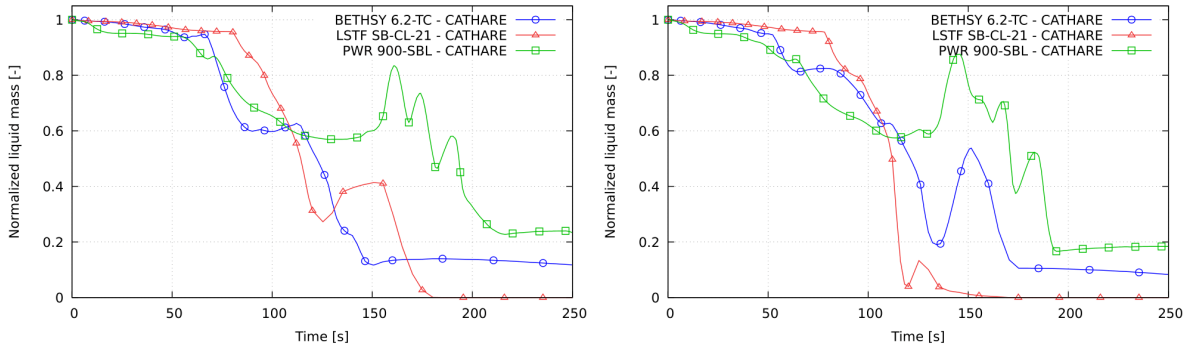

Figure 14. Liquid mass plugged in IL of the intact loop(s) (left), and broken loop (right) – predicted by CATHARE

The LSP/LSC phenomenon has been observed experimentally on all the IL of the facilities. However, the code results predict the LSP on a single IL. A certain randomness of the LSC process has been observed, which makes it is difficult to predict by the codes (Hwang et al., 2019). Some experimental tests revealed an asymmetry between loops, while repeatable tests revealed LSC in different loops. These investigations also revealed that the IL were not completely cleared for some tests, as seen on BETHSY and the PWR but not on LSTF. To better analyse these LSC phenomena, one should look at the pressure difference between the two thermodynamically independent systems on either side of the plug. Figure 15 shows that the pressure difference is greater on LSTF than on BETHSY and in the PWR. It should be noted that the remaining mass in non-cleared loops reduces the collapsed level in the core and thus has an effect on the PCT.

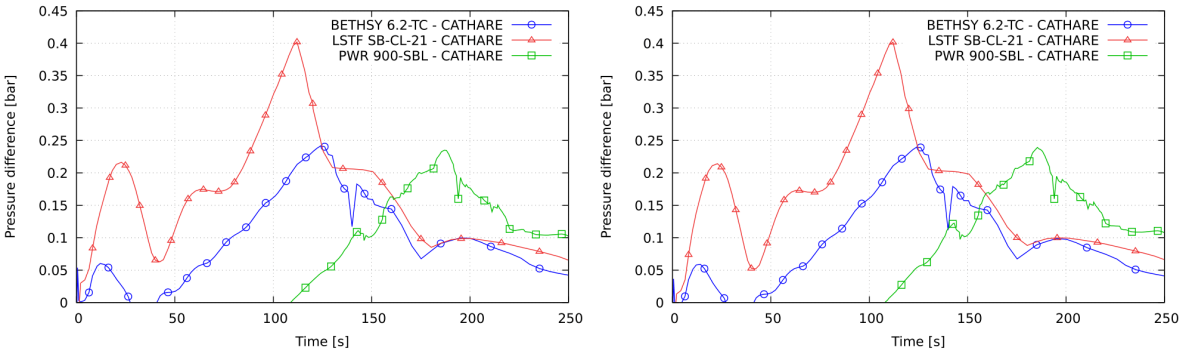

Figure 15. Pressure difference between HL inlet and CL outlet – intact loop(s) (left), broken loop (right) – predicted by CATHARE

Several effects can explain the asymmetric behaviour:

- There is no significant differences between intact and broken loop pressure difference (see Figure 15) since it is the pressure difference between the upper plenum and top of downcomer.
- Differences in IL height between BETHSY and LSTF are observed. The difference between the elevation of the horizontal CL and the bottom of the IL is 2.2 m on BETHSY and 3.7 m on LSTF.
- The heat transfer coefficient in the SG tubes may slightly differ between SG, resulting in more or less condensate liquid falling in the IL.
- The first loop to be cleared may equalize pressures before the other(s) can be cleared. The predicted differences between loops is visible in the liquid mass in IL (see Figure 14). They show that at the time a first loop is cleared, the other still did not fully clear and some water flows back to it. Small differences in initial fluid mass in the IL can result in different behaviour.

The depressurization of the RCM phase is investigated using the FSA method applied to mass and pressure (VRC) equations, for the primary system control volume. Table 11 shows the main parameters of the RCM phase.

Table 11. Main parameters of the RCM phase – predicted by CATHARE

	BETHSY	LSTF	PWR
Initial primary mass $M_{1,0}$	914 kg	2 536 kg	98 237 kg
Phase duration Δt_{RCM}	71 s	60 s	76 s
Primary mass difference ΔM_1	324 kg	627 kg	32 410 kg
Pressure difference ΔP_{RCM}	0.58 MPa	0.96 MPa	0.38 MPa
Averaged mass flow rate at the break $\overline{\dot{M}}_{break}$	5.12 kg/s	12.61 kg/s	447.71 kg/s
Averaged core power $\overline{W}_{core}$	$1.62 \cdot 10^6$ W	$5.49 \cdot 10^6$ W	$9.09 \cdot 10^7$ W
Averaged core power ratio (facilities/PWR)	1/56	1/17	-
Averaged SG tubes heat exchanges $\overline{W}_{SG}$	$9.16 \cdot 10^6$ W	$2.77 \cdot 10^6$ W	$3.54 \cdot 10^7$ W
Averaged primary wall heat exchanges $\overline{W}_{1,ow}$	$1.21 \cdot 10^5$ W	$8.37 \cdot 10^4$ W	$1.03 \cdot 10^7$ W
Averaged liquid temperature $\overline{T}_{1,l}$	290.8 °C	291.3 °C	285.9 °C
Averaged vapour temperature $\overline{T}_{1,v}$	297.8 °C	293.6 °C	287.9 °C

Table 12 displays the values of the effect metrics for the mass equation $\Omega_{\dot{M},j}$ and the pressure equation $\Omega_{\dot{P},j}$ for the RCM phase of the primary system.

Table 12. Effect metrics of the primary system during the RCM phase

		BETHSY	LSTF	PWR
Rate of mass change due to the contribution by:				
Liquid flow rate leaving the primary system through the break	$\Omega_{\dot{M}_{l,break}}$	**-1.000**	**-1.000**	**-1.000**
Vapour flow rate leaving the primary system through the break	$\Omega_{\dot{M}_{v,break}}$	**-0.218**	**-0.293**	**-0.219**
Rate of pressure change due to the contribution by:				
Liquid volume flow rate leaving the primary system through the break	$\Omega_{\dot{P},Q_{l,break}}$	**-0.245**	**-0.193**	**-0.229**
Vapour volume flow rate leaving the primary system through the break	$\Omega_{\dot{P},Q_{v,break}}$	**-1.000**	**-1.000**	**-1.000**
Thermal expansion/contraction by wall-liquid heat transfers in the core	$\Omega_{\dot{P},Q_{wl,core}}$	0.002	0.002	0.002
Thermal expansion/contraction by wall-vapour heat transfers in the core	$\Omega_{\dot{P},Q_{wv,core}}$	**0.138**	0.020	0.023
Volume change by wall boiling or condensation in the core	$\Omega_{\dot{P},Q_{wi,core}}$	**0.997**	**0.796**	**0.727**
Thermal expansion/contraction by interface-liquid heat transfers in the core	$\Omega_{\dot{P},Q_{il,core}}$	-0.001	-0.002	-0.002
Thermal expansion/contraction by interface-vapour heat transfers in the core	$\Omega_{\dot{P},Q_{iv,core}}$	**-0.094**	-0.041	-0.010
Volume change by vaporization or condensation by interfacial transfers in the core	$\Omega_{\dot{P},Q_{i,core}}$	**0.084**	**0.073**	**0.055**
Thermal expansion/contraction by wall-liquid heat transfers in SG tubes	$\Omega_{\dot{P},Q_{wl,SG}}$	-0.027	-0.030	-0.008
Thermal expansion/contraction by wall-vapour heat transfers in SG tubes	$\Omega_{\dot{P},Q_{wv,SG}}$	0.000	0.000	0.002
Volume change by wall boiling or condensation in SG tubes	$\Omega_{\dot{P},Q_{wi,SG}}$	-0.006	0.001	0.006
Thermal expansion/contraction by interface-liquid heat transfers in the SG tubes	$\Omega_{\dot{P},Q_{il,SG}}$	0.027	0.029	0.011
Thermal expansion/contraction by interface-vapour heat transfers in the SG tubes	$\Omega_{\dot{P},Q_{iv,SG}}$	0.007	0.015	0.005

Volume change by vaporization or condensation by interfacial transfers in the SG tubes	$\Omega_{\dot{P},Q_{i,SG}}$	**-0.624**	**-0.634**	**-0.285**
Thermal expansion/contraction by wall-liquid heat transfers in the primary system*	$\Omega_{\dot{P},Q_{owl}}$	-0.001	-0.001	0.001
Thermal expansion/contraction by wall-vapour heat transfers in the primary system*	$\Omega_{\dot{P},Q_{owv}}$	0.014	0.002	0.008
Volume change by wall boiling or condensation in the primary system*	$\Omega_{\dot{P},Q_{owi}}$	**0.069**	0.044	0.044
Thermal expansion/contraction by interface-liquid heat transfers in the primary system*	$\Omega_{\dot{P},Q_{il,ov}}$	-0.002	-0.006	-0.002
Thermal expansion/contraction by interface-vapour heat transfers in the primary system*	$\Omega_{\dot{P},Q_{iv,ov}}$	-0.045	0.018	-0.010
Volume change by vaporization or condensation by interfacial transfers in the primary system*	$\Omega_{\dot{P},Q_{i,ov}}$	**0.081**	**0.115**	**0.065**

*(except SG tubes and fuel rods)

The liquid mass flow rate at the break remains the dominant effect metric on the rate of mass change. The RCM phase is a transition phase in which the primary system gradually loses liquid. As a result, the break vapour mass flow rate effect metric is higher than in the NC phase (BETHSY: -0.218; LSTF: -0.293; PWR: -0.219).

The vapour volume flow rate at the break is now the dominant process in terms of effect metric related to rate of pressure change. Volume change by condensation from interfacial transfers in SG tubes also contributes to depressurization. It appears to be lower in the PWR (-0.285) than in the facilities (BETHSY: -0.624; LSTF: -0.634). The predicted liquid volume flow rate at the break is still significant, but its importance diminishes as the transient progresses. It is also higher on BETHSY (-0.245) than in LSTF (-0.193) and the PWR (-0.229). The volume change caused by wall-boiling in the core compensates partially for the depressurization. This term also appears to be relatively higher in BETHSY (0.997) than in LSTF (0.796) and the PWR (0.727). It should be noted that the effect metric related to thermal expansion by wall-vapour in the core is influent on BETHSY (0.138), whereas it is negligible on LSTF (0.020) and PWR (0.023). This is due to the prediction of a rather long core dry-out period with wall and vapour superheating in BETHSY compared to the predicted core uncovery in LSTF and in PWR. However, the core dry-out duration is over-predicted in BETHSY calculation and under-predicted in the LSTF calculation (see Figure 6 and Figure 7).

4.6. Results of the a posteriori scaling analysis of the High-Quality Mixture Discharge (HQMD) phase

The HQMD phase is characterized by a void fraction at the break very that is close to 1, as shown in Figure 13. The crossing of the primary and secondary pressures is the HQMD phase bifurcating event. This is a significant event for the remainder of the transient because it is at this point that the SG cease to function as heat sinks. Figure 16 depicts the predicted and measured pressure reversal, which occurs earlier and at higher pressure in the facilities than in the PWR since the mass inventory in the PWR remains higher due to a lower break flow rate resulting from a lower pressure plateau. Because of the discharge of vapour through the break, the primary pressure begins to fall again after the plateau of the NC and RCM phases. Given the absence of HPIS, the primary mass inventory continues to decline.

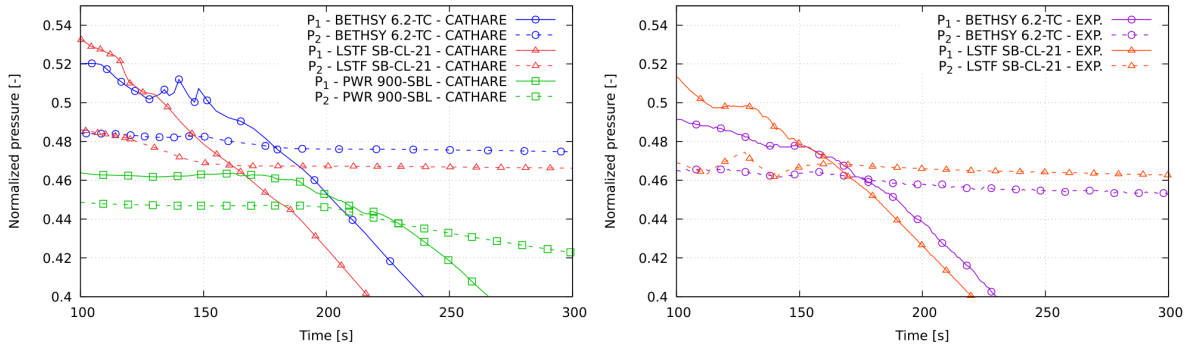

Figure 16. Primary and secondary pressures at the HQMD bifurcating event – predicted by CATHARE (left), experimental results (right)

The depressurization of the HQMD phase is investigated using the FSA method applied to mass and pressure (VRC) equations, for the primary system control volume. Table 13 shows the main parameters of the HQMD phase.

Table 13. Main parameters of the HQMD phase – predicted by CATHARE

	BETHSY	LSTF	PWR
Initial primary mass $M_{l,0}$	580 kg	1 882 kg	65 483 kg
Phase duration Δt_{HQMD}	175 s	175 s	140 s
Primary mass difference ΔM_l	224 kg	664 kg	20 428 kg
Pressure difference ΔP_{HQMD}	3.01 MPa	2.94 MPa	2.69 MPa
Averaged mass flow rate at the break $\overline{\dot{M}}_{break}$	1.43 kg/s	3.90 kg/s	163.12 kg/s
Averaged core power $\overline{W}_{core}$	$9.02 \cdot 10^5$ W	$2.89 \cdot 10^6$ W	$8.15 \cdot 10^7$ W
Averaged core power ratio (facilities/PWR)	1/90	1/28	-
Averaged SG tubes heat exchanges $\overline{W}_{SG}$	$8.45 \cdot 10^4$ W	$2.50 \cdot 10^5$ W	$4.27 \cdot 10^6$ W
Averaged primary wall heat exchanges $\overline{W}_{l,ow}$	$5.51 \cdot 10^5$ W	$8.78 \cdot 10^5$ W	$2.94 \cdot 10^7$ W
Averaged liquid temperature $\overline{T}_{l,l}$	271.2 °C	270.7 °C	269.3 °C
Averaged vapour temperature $\overline{T}_{l,v}$	283.5 °C	276.9 °C	272.2 °C

Table 14 displays the values of the effect metrics for the mass equation $\Omega_{\dot{M},j}$ and the pressure equation $\Omega_{\dot{P},j}$ for the HQMD phase of the primary system.

Table 14. Effect metrics of the primary system during the HQMD phase

		BETHSY	LSTF	PWR
Rate of mass change due to the contribution by:				
Liquid flow rate leaving the primary system through the break	$\Omega_{\dot{M}_{l,break}}$	-0.043	**-0.065**	**-0.533**
Vapour flow rate leaving the primary system through the break	$\Omega_{\dot{M}_{v,break}}$	**-1.000**	**-1.000**	**-1.000**
Rate of pressure change due to the contribution by:				
Liquid volume flow rate leaving the primary system through the break	$\Omega_{\dot{P},Q_{l,break}}$	-0.001	-0.002	-0.019
Vapour volume flow rate leaving the primary system through the break	$\Omega_{\dot{P},Q_{v,break}}$	**-1.000**	**-1.000**	**-1.000**
Thermal expansion/contraction by wall-liquid heat transfers in the core	$\Omega_{\dot{P},Q_{wl,core}}$	0.001	0.000	0.001
Thermal expansion/contraction by wall-vapour heat transfers in the core	$\Omega_{\dot{P},Q_{wv,core}}$	0.001	0.000	0.001
Volume change by wall boiling or condensation in the core	$\Omega_{\dot{P},Q_{wi,core}}$	**0.362**	**0.322**	**0.474**
Thermal expansion/contraction by interface-liquid heat transfers in the core	$\Omega_{\dot{P},Q_{il,core}}$	-0.001	-0.001	-0.002

Thermal expansion/contraction by interface-vapour heat transfers in the core	$\Omega_{\dot{P},\dot{Q}_{iv,core}}$	0.001	0.002	0.001
Volume change by vaporization or condensation by interfacial transfers in the core	$\Omega_{\dot{P},\dot{Q}_{i,core}}$	0.042	0.048	**0.061**
Thermal expansion/contraction by wall-liquid heat transfers in SG tubes	$\Omega_{\dot{P},\dot{Q}_{wl,SG}}$	0.000	0.000	0.000
Thermal expansion/contraction by wall-vapour heat transfers in SG tubes	$\Omega_{\dot{P},\dot{Q}_{wv,SG}}$	**0.059**	**0.066**	**0.099**
Volume change by wall boiling or condensation in SG tubes	$\Omega_{\dot{P},\dot{Q}_{wi,SG}}$	0.014	0.004	**0.059**
Thermal expansion/contraction by interface-liquid heat transfers in the SG tubes	$\Omega_{\dot{P},\dot{Q}_{il,SG}}$	0.000	0.000	0.001
Thermal expansion/contraction by interface-vapour heat transfers in the SG tubes	$\Omega_{\dot{P},\dot{Q}_{iv,SG}}$	0.001	0.000	-0.021
Volume change by vaporization or condensation by interfacial transfers in the SG tubes	$\Omega_{\dot{P},\dot{Q}_{i,SG}}$	0.000	0.000	-0.031
Thermal expansion/contraction by wall-liquid heat transfers in the primary system*	$\Omega_{\dot{P},\dot{Q}_{owl}}$	0.002	0.001	0.001
Thermal expansion/contraction by wall-vapour heat transfers in the primary system*	$\Omega_{\dot{P},\dot{Q}_{owv}}$	0.042	0.009	0.009
Volume change by wall boiling or condensation in the primary system*	$\Omega_{\dot{P},\dot{Q}_{owi}}$	**0.140**	**0.104**	**0.082**
Thermal expansion/contraction by interface-liquid heat transfers in the primary system*	$\Omega_{\dot{P},\dot{Q}_{il,ov}}$	-0.005	-0.006	-0.006
Thermal expansion/contraction by interface-vapour heat transfers in the primary system*	$\Omega_{\dot{P},\dot{Q}_{iv,ov}}$	-0.034	0.017	0.006
Volume change by vaporization or condensation by interfacial transfers in the primary system*	$\Omega_{\dot{P},\dot{Q}_{i,ov}}$	**0.205**	**0.206**	**0.225**

*(except SG tubes and fuel rods)

The pressure reversal results from an almost vapour flow at the break, as demonstrated by the dominant effect metric related to the break volume flow rate for the BETHSY and LSTF facilities. Figure 13 shows that the void fraction at the break is lower on the PWR than on the facilities at the start of the HQMD phase. Because of the different pump behaviours, the effect metric related to the liquid mass flow rate is distorted on the facilities (BETHSY: -0.043; LSTF: -0.065) compared to PWR (-0.533).

The vapour volume flow rate at the break is the dominant effect metric related to the rate of pressure change. It dominates the other phenomena, which explains the second depressurization after the pressure plateau (see Figure 4). When compared to the RCM phase, the effect metric related to volume change caused by wall-boiling in the core has decreased. The core boiling is then no longer sufficient to compensate for the fluid volume lost at the break. However, the core boiling is still slightly influential and its impact on the PWR (0.474) is greater than on the facilities (BETHSY: 0.362; LSTF: 0.322). Because of the decreased pressure, wall-boiling and vaporization by flashing in the primary system are slightly higher than in the NC and RCM phases. Given the void fraction close to 1, the effect metric related to the liquid volume flow rate at the break is now negligible (BETHSY: -0.001; LSTF: -0.002; PWR: -0.019). Thermal contraction by wall-liquid in SG tubes heat transfers is now zero given the absence of liquid. Thermal expansion caused by wall-vapour in SG tubes heat transfers begins to have a minor impact on pressure (BETHSY: 0.059; LSTF: 0.066; PWR: 0.099). Likewise, volume change by wall-boiling (BETHSY: 0.140; LSTF: 0.104; PWR: 0.082) and by vaporization (BETHSY: 0.205; LSTF: 0.206; PWR: 0.225) in the primary system become influent during HQMD phase.

4.7. Results of the a posteriori scaling analysis of the Reactor Refilling (RR) phase

The RR phase starts with the accumulator injection, triggered when the primary pressure drops below 4.2 MPa. The primary circuit mass inventory is at its minimum at the start of this phase (see Figure 3). The code predicts a second core uncovery, which is observed experimentally on BETHSY and not on LSTF. It is smaller than the first uncovery. The BETHSY second PCT occurs at 92% of the core height

and reaches a temperature of 286 °C (324 °C experimentally). The primary system refills and the mass inventory grows after a few seconds.

Figure 17 depicts the accumulator liquid mass. The injection behaviour of the three systems is observed to be different. After 520 seconds of transient, several stages of injections are predicted in BETHSY calculation. These stages are not detected experimentally and are thus code-induced errors. A single stage is observed at 480 seconds in LSTF predictions, but it lasts much longer in the code predictions than experimentally. The PWR predictions show more stages, but they are much less intense. Figure 18 depicts the core-collapsed level during the RR phase. Predicted liquid level oscillations in the BETHSY core are found to correspond to the injections stages. It should be noted that both BETHSY and the PWR have two accumulators on the two intact CL. On the other hand, LSTF has only one accumulator on the broken CL.

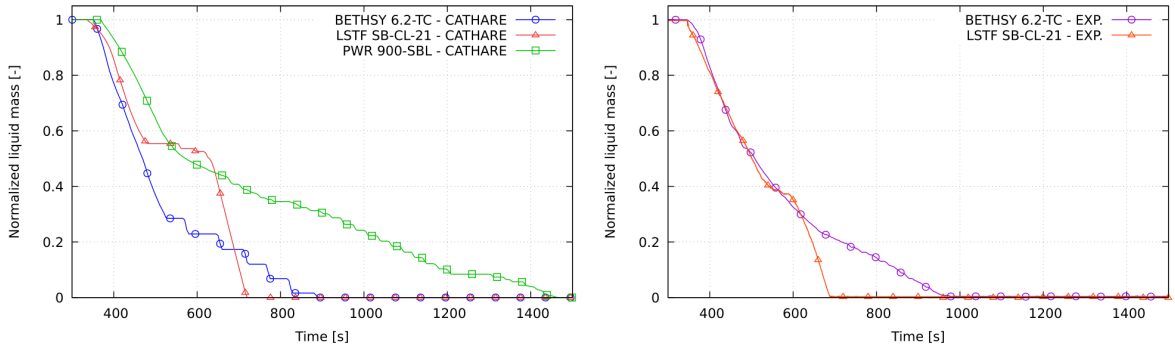

Figure 17. Accumulator liquid mass – predicted by CATHARE (left), experimental results (right)

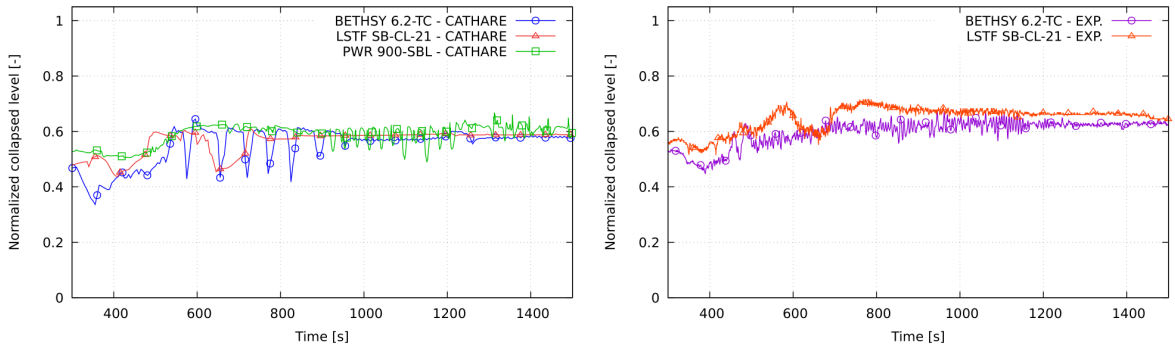

Figure 18. Core-collapsed level during the RR – predicted by CATHARE (left), experimental results (right)

The depressurization of the RR phase is investigated using the FSA method applied to mass and pressure (VRC) equations, for the primary system control volume. Table 15 shows main parameters of the RR phase.

Table 15. Main parameters of the RR phase – predicted by CATHARE

	BETHSY	LSTF	PWR
Initial primary mass $M_{1,0}$	335 kg	1 215 kg	45 045 kg
Phase duration Δt_{RR}	539 s	384 s	1098 s
Primary mass difference ΔM_1	247 kg	818 kg	24 331 kg
Pressure difference ΔP_{RR}	2.67 MPa	2.85 MPa	3.28 MPa
Averaged mass flow rate at the break $\bar{\dot{M}}_{break}$	0.46 kg/s	1.54 kg/s	47.91 kg/s
Averaged accumulator mass flow rate $\bar{\dot{M}}_{l.acc.}$	0.95 kg/s	3.71 kg/s	50.00 kg/s
Averaged core power $\bar{W}_{core}$	$6.06 \cdot 10^5$ W	$1.85 \cdot 10^6$ W	$5.21 \cdot 10^7$ W
Averaged core power ratio (facilities/PWR)	1/86	1/28	-
Averaged SG tubes heat exchanges $\bar{W}_{SG}$	$1.11 \cdot 10^5$ W	$2.31 \cdot 10^5$ W	$1.41 \cdot 10^7$ W

Averaged primary wall heat exchanges $\overline{W}_{l,ow}$	$5.59 \cdot 10^5$ W	$2.25 \cdot 10^6$ W	$2.88 \cdot 10^7$ W
Averaged liquid temperature $\overline{T}_{l,l}$	207.1 °C	216.7 °C	186.2 °C
Averaged vapour temperature $\overline{T}_{l,v}$	265.6 °C	248.9 °C	227.9 °C

Table 16 displays the values of the effect metrics for the mass equation $\Omega_{\dot{M},j}$ and the pressure equation $\Omega_{\dot{P},j}$ for the RR phase of the primary system.

Table 16. Effect metrics of the primary system during the RR phase

		BETHSY	LSTF	PWR
Rate of mass change due to the contribution by:				
Liquid flow rate leaving the primary system through the break	$\Omega_{\dot{M}_{l,break}}$	-0.022	-0.002	**-0.438**
Vapour flow rate leaving the primary system through the break	$\Omega_{\dot{M}_{v,break}}$	**-0.464**	**-0.414**	**-0.521**
Liquid flow rate entering the primary system thanks to accumulator discharge	$\Omega_{\dot{M}_{l,acc.}}$	**1.000**	**1.000**	**1.000**
Rate of pressure change due to the contribution by:				
Liquid volume flow rate leaving the primary system through the break	$\Omega_{\dot{P},Q_{l,break}}$	0.000	0.000	-0.005
Vapour volume flow rate leaving the primary system through the break	$\Omega_{\dot{P},Q_{v,break}}$	**-1.000**	**-1.000**	**-0.997**
Thermal expansion/contraction by wall-liquid heat transfers in the core	$\Omega_{\dot{P},Q_{wl,core}}$	0.000	0.000	0.000
Thermal expansion/contraction by wall-vapour heat transfers in the core	$\Omega_{\dot{P},Q_{wv,core}}$	0.001	0.000	0.000
Volume change by wall boiling or condensation in the core	$\Omega_{\dot{P},Q_{wi,core}}$	**0.627**	**0.421**	**0.990**
Thermal expansion/contraction by interface-liquid heat transfers in the core	$\Omega_{\dot{P},Q_{il,core}}$	0.000	-0.001	0.000
Thermal expansion/contraction by interface-vapour heat transfers in the core	$\Omega_{\dot{P},Q_{iv,core}}$	0.001	0.001	0.001
Volume change by vaporization or condensation by interfacial transfers in the core	$\Omega_{\dot{P},Q_{i,core}}$	**0.072**	**0.083**	**0.106**
Thermal expansion/contraction by wall-liquid heat transfers in SG tubes	$\Omega_{\dot{P},Q_{wl,SG}}$	0.000	0.000	0.000
Thermal expansion/contraction by wall-vapour heat transfers in SG tubes	$\Omega_{\dot{P},Q_{wv,SG}}$	**0.199**	**0.161**	**0.581**
Volume change by wall boiling or condensation in SG tubes	$\Omega_{\dot{P},Q_{wi,SG}}$	**0.051**	0.000	**1.000**
Thermal expansion/contraction by interface-liquid heat transfers in the SG tubes	$\Omega_{\dot{P},Q_{il,SG}}$	0.000	0.000	0.001
Thermal expansion/contraction by interface-vapour heat transfers in the SG tubes	$\Omega_{\dot{P},Q_{iv,SG}}$	-0.001	0.000	**-0.084**
Volume change by vaporization or condensation by interfacial transfers in the SG tubes	$\Omega_{\dot{P},Q_{i,SG}}$	0.001	0.000	**-0.269**
Thermal expansion/contraction by wall-liquid heat transfers in the primary system*	$\Omega_{\dot{P},Q_{owl}}$	0.002	0.004	0.001
Thermal expansion/contraction by wall-vapour heat transfers in the primary system*	$\Omega_{\dot{P},Q_{owv}}$	**0.088**	0.029	**0.065**
Volume change by wall boiling or condensation in the primary system*	$\Omega_{\dot{P},Q_{owi}}$	**0.373**	**0.286**	**0.255**
Thermal expansion/contraction by interface-liquid heat transfers in the primary system*	$\Omega_{\dot{P},Q_{il,ov}}$	0.001	0.000	0.000
Thermal expansion/contraction by interface-vapour heat transfers in the primary system*	$\Omega_{\dot{P},Q_{iv,ov}}$	**-0.073**	-0.001	-0.020
Volume change by vaporization or condensation by interfacial transfers in the primary system*	$\Omega_{\dot{P},Q_{i,ov}}$	-0.049	-0.017	-0.014

Thermal expansion by liquid flow entering the primary system thanks to accumulator discharge	$\Omega_{\dot{P},Q_{l,acc.}}$	0.020	0.029	0.012
Thermal expansion by condensation due to the liquid flow rate entering the primary system thanks to accumulator discharge	$\Omega_{P,Q_{cond,l,acc.}}$	-0.005	-0.008	-0.002

*(except SG tubes and fuel rods)

The liquid mass flow rate provided by the accumulator discharge is the dominant process in terms of effect metrics on the rate of mass change during the RR phase. The distribution of liquid (BETHSY: -0.022; LSTF: -0.002; PWR: -0.438) and vapour (BETHSY: -0.464; LSTF: -0.414; PWR: -0.521) mass flow rates at the break, on the other hand, is not evenly distributed between the facilities and the PWR. The mass flow rate at the break, particularly the liquid flow rate, is proportionally higher in the PWR than in the facilities.

The behaviour in the facilities seems to be distorted compared to the PWR, as shown in Figure 17. The longer duration of the PWR accumulator injection alters the process behaviour of this phase. The vapour volume flow rate at the break is the dominant effect metric contributing to the depressurization. Volume change by wall-boiling in the core plays a dominant role in compensating for the depressurization, but its impact is significantly higher in the PWR (0.990) than in the facilities (BETHSY: 0.627; LSTF: 0.421). Similarly, thermal expansion by interface-vapour heat transfers (BETHSY: 0.199; LSTF: 0.083; PWR: 0.581) and volume change by wall-boiling (BETHSY: 0.051; LSTF: 0.000; PWR: 1.000) in the SG tubes occur with higher intensity in the PWR than in the facilities. The liquid discharged from the PWR accumulators condenses some vapour. There is some vaporization in the system hot spots, the core and the SG tubes, slowing the system depressurization. It should also be noted that volume change by wall-boiling in the primary system now plays a significant role (BETHSY: 0.373; LSTF: 0.286; PWR: 0.255). It is slightly higher in the facilities, particularly in BETHSY, due to the ratio between the primary circuit exchange surface and the primary volume.

The significant distortions observed during the RR phase on the PWR compared to the facilities are investigated. Sensitivity studies have been carried out regarding several parameters of the accumulator injection process. The simplest accumulator model of CATHARE is modelled as a fluid injection sub-module using a constant expansion coefficient for the nitrogen without modelling the thermal exchanges with accumulator walls. Thermal exchanges between accumulator walls and the nitrogen are higher on scaled facilities than in the PWR. An isentropic expansion coefficient γ equal to 1.4 has been used in PWR calculation (corresponding to zero thermal exchanges with walls) whereas values of 1.0 and 1.15 have been used respectively for BETHSY and LSTF. These expansion coefficients values were initially calculated to better fit the experimental results, as used with the fluid injection sub-module. A more accurate modelling of the BETHSY accumulators is used to investigate the differences in the discharge behaviour between the facilities and the PWR. This modelling is based on a 0-D module for the accumulator tank and a 1-D module for the discharge line. Thus, wall exchanges are modelled and calculated instead of relying on an estimated mean expansion coefficient.

Figure 19 depicts the accumulator discharge behaviours of BETHSY and the PWR:
- Predicted by CATHARE, with an expansion coefficient calculated to better fit with BETHSY experimental results (i.e. with the fluid injection sub-module).
- Predicted by CATHARE, using a more accurate accumulator modelling (i.e. with 0-D and 1-D modules), which calculates heat exchanges between nitrogen and walls.
- From the BETHSY experimental results.
- Predicted by CATHARE, assuming isentropic expansion for the PWR.

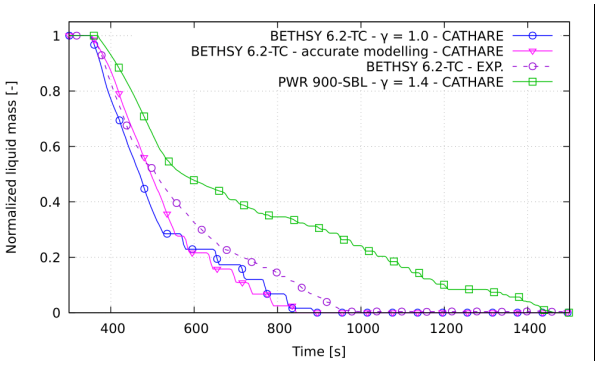

Figure 19. Investigation of accumulator liquid mass distortions – predicted by CATHARE

The two BETHSY accumulator modelling show the same trend, which is close to the experimental trend with several closure and opening of the valve not seen in BETHSY. The difference between BETHSY and the reactor is more significant and is attributed to the distorted parameters of the accumulators: increased metallic thermal capacity and increased ratio between the wall exchange surface to the volume. As a result, more heat is released from the wall to the nitrogen, the accumulator pressure drops more slowly, and the discharge flow rate is higher than in the reactor. As a result, the accumulator discharge is faster on the facilities.

4.8. Modification of PWR pumps behaviour and core power decay law

An analysis is performed here to validate previous hypothesis about the observed distortions between the PWR and the facilities. The PWR dataset is modified to reflect the conditions of the facilities. Figure 20 depicts significant evolutions influenced by these changes. Given that this is the reference reactor, a comparison is made between the original PWR dataset and the BETHSY 6.2-TC test. The parameters under consideration are:

- The core power decay laws of the facilities, which differs from the PWR at the first instants of the transient. This can be seen from the averaged core power ratio between the facilities and the PWR. In the SBD phase, these ratios are 1/706 and 1/242, respectively for BETHSY and LSTF, and drop to 1/64 and 1/22 in the NC phase. These cause different behaviours, most notably boiling in the core and the amount of vapour in the primary circuit. The JAERI conservative decay power curve is imposed on the PWR on the "Modif. power" curves. The initial power is also scaled to 10% of the original nominal value, just like the facilities.
- The impact of pump behaviour on PWR compared to facilities. The inertia of the PWR pumps alters the natural circulation phase, as seen in BETHSY and LSTF, where the pumps are stopped almost immediately. The transient is simulated on the PWR without pump inertia on the "Modif. pumps" curves in the same way that it is in the facilities.

Both modifications are taken into account on the "Modif. power/pumps" curves.

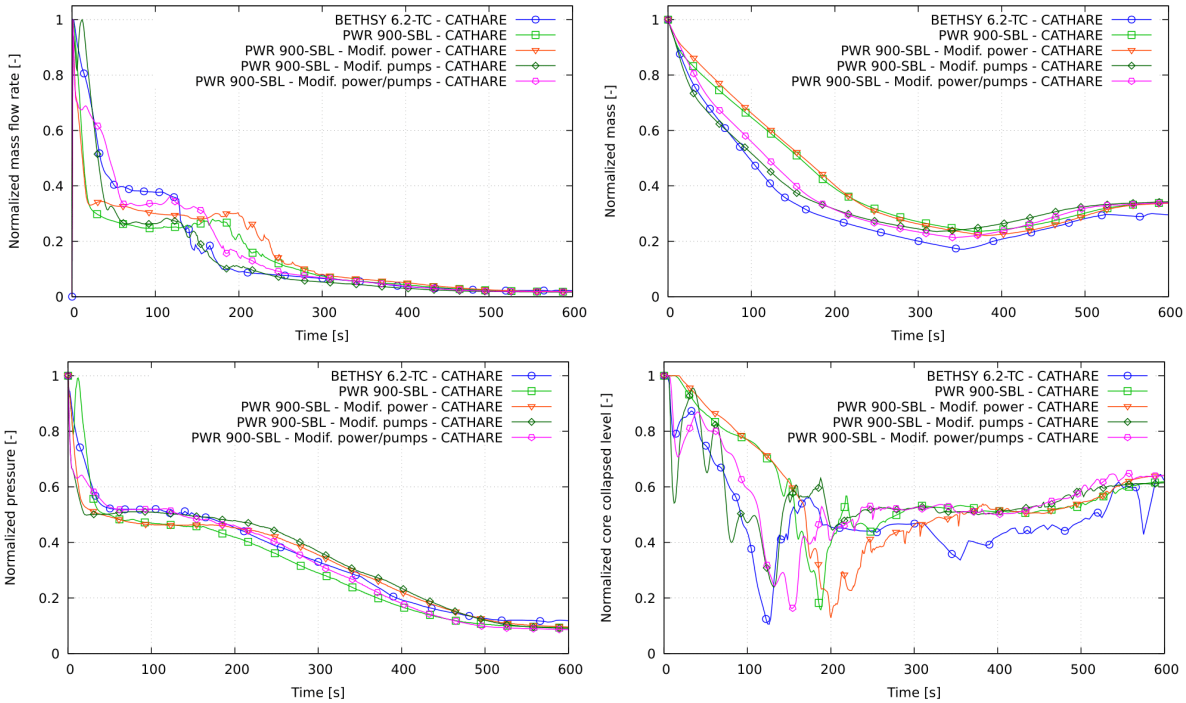

Figure 20. Comparison of major transient evolutions – break mass flow rate (top left), primary mass inventory (top right), primary pressure (bottom left), core-collapsed level (bottom right) – predicted by CATHARE

These changes have an impact on the main evolutions in the PWR transient, as shown in Figure 20. It is observed that:

- The power correction brings the evolutions of the PWR break mass flow rate (Figure 20 (top left)) and the primary pressure (Figure 20 (bottom left)) closer to BETHSY evolutions during the plateau in the NC and the RCM phases.
- The changes in the pumps behaviour bring the PWR evolutions significantly closer to the BETHSY evolutions during the SBD and the HQMD phases. The mass flow rate at the break (Figure 20 (top left)), primary mass inventory (Figure 20 (top right)) and primary pressure (Figure 20 (bottom left)) during the SBD are closer to BETHSY behaviour. This correction also removes the PWR core uncovery temporal shift when compared to BETHSY. This correction also reduces the temporal shift that was observed on major transient phenomena, such as the first core uncovery in Figure 20 (bottom right).

5. Conclusions

A scaling analysis is performed on a cold leg SB-LOCA transient comparing two IETs of a counterpart test (D'Auria et al., 1992; Kumamaru et al., 1992) and a PWR simulation:
- The 6.2-TC test performed on the French BETHSY facility (Equipe BETHSY, 1990).
- The SB-CL-21 test performed on the Japanese LSTF-ROSA facility (The ROSA-V Group, 1985).
- A full-scale model of a Framatome commercial reactor.

The FSA method is applied here to primary mass and primary pressure equations. The term values for those equations are here evaluated using CATHARE code simulations. The SB-LOCA transient is divided into five phases that are applied to the primary system and the pressurizer volumes. The purpose of this work is to provide an analysis of the distortions between scale-reduced facilities and full-scale PWR. Another objective is to show how system codes that have reached a reasonable level of maturity and confidence may support and improve the application of scaling methods.

The formulation of the pressurizer and primary circuit pressure equations as volume rate of change equations gives each contributor a clear physical meaning. Pressurization can be caused by any fluid volume source (or sink) (respectively depressurization). Any amount of heating (or cooling) contributes to pressurization (respectively depressurization). Because the volume is constant, any imbalance in heating, cooling, fluid volume sources and sinks is compensated by a fluid volume expansion or contraction caused by a decrease or increase in pressure.

The scaling analysis results, along with the evolution and differences in the effect metrics of the three systems, allow us to detect the presence of distortions:
- In the pressurizer emptying, the behaviour of the predicted LSTF pressurizer differs from the predicted BETHSY pressurizer due to its design difference (full height for BETHSY and a reduced height in LSTF).
- The facilities seem to be distorted since the predicted vapour volume flow rate leaving the pressurizer are smaller than in the PWR simulation. However this may be related to an oversimplified 0-D two-node pressurizer modelling with CATHARE, which cannot predict very precisely the void fraction entrained in the expansion line.
- During the subcooled blowdown phase, significant distortions between the facilities and the PWR are observed in the primary system due to pump behaviour and power evolution differences. Higher volume change by wall heat transfers in the PWR core and SG tubes are observed compared to the facilities just reflecting the fact that core power is truncated at 10% and 11% in experiments. The initial pump produces only 10% of nominal flow rate in experiments and pump speed rapidly decreases to zero. These two differences impact the loop flow rate and the break quality and flow rate.
- The natural circulation phase is temporally distorted because of the PWR pumps behaviour in comparison to the facilities. These distortions are transferred to the RCM, HQMD and RR phases of the transient.
- The reactor refilling phase also differs significantly between the facilities and the PWR. It is demonstrated that scaling effects on heat transfers between accumulator walls and nitrogen can drastically change the discharge duration. These results indicate that choices in the basic design of ITFs can have a notable impact on phenomena behaviour throughout the transient.
- Some distortions are found in the wall heat transfers and the wall-boiling/condensation phenomena between the facilities and the PWR, but also between BETHSY and LSTF. These discrepancies are due to the overestimated wall thermal mass and thermal inertia, and overestimated wall heat transfer area in the scaled experiments (except for the fuel rods and SG tubes). These are unavoidable scale effect directly caused by the power-to-volume scaling method used in the design of these facilities.
- The LSP and LSC phenomena are still difficult to predict by the calculation codes. Further research will be conducted to perform a scaling analysis on the IL in order to better understand these phenomena and the processes or scale effects that influence them.

Using the FSA scaling method, it is possible to conclude that using a mature and extensively validated system code – here, the CATHARE code – reduces the impact of the assumptions made to evaluate the

terms of the equations for the scaling analysis. The code actually provides more precision by averaging these values rather than relying on estimates at the phase boundaries. Scaling analyses can now be performed using system codes. As demonstrated, scaling tools such as equations at the system level can also support the improvement of code modelling by identifying code errors or sensitive phenomena.

It would be interesting to extend this work at the component and local scale analysis of the counterpart test.

An analysis of similar tests performed in facilities having different scaling methods such as full-height or reduced-height will also be considered. These studies will eventually allow the implementation of a scaling analysis module in the CATHARE code which allows an easy plotting of any terms of the scaling equations at system/component level.

Acknowledgements

This work has been carried out in the framework of the SIMULATION CEA/DES program. The present work contains findings that are produced within the OECD/NEA ROSA-2 Project. The author is grateful to the Management Board of this project for its consent to this publication. The author is also grateful to the CEA colleagues for their support and help during the experiment analysis and the CATHARE modelling.

References

Bestion, D., 2020. About phenomena identification in a PIRT, in: NURETH-18. Portland, USA.

Bestion, D., 1990. The physical closure laws in the CATHARE code. Nuclear Engineering and Design 124, 229–245. https://doi.org/10.1016/0029-5493(90)90294-8

Bestion, D., D'Auria, F., Lien, P., Nakamura, H., 2017. A state-of-the-art report on scaling in system thermal hydraulics applications to nuclear reactor safety and design. OECD/NEA/CSNI/R(2016)14.

Ciechocki, A., Carnevali, S., Bestion, D., Rossi, L., 2022. Application of the FSA scaling method to the LSTF ROSA 1.2 test and comparison to an application of the H2TS method, in: NURETH-19.

Cummins, W.E., Corletti, M.M., Schulz, T.L., 2003. Westinghouse AP1000 advanced passive plant. Proceedings of ICAPP '03 236, 1547–1557. https://doi.org/10.1016/j.nucengdes.2006.03.049

D'Auria, F., Ferri, R., Galassi, G.M., Sugaroni, F., 1992. Evaluation of the data base from the small break LOCA counterpart tests performed in LOBI, SPES, BETHSY and LSTF facilities. Dipartimento Costruzioni Meccaniche E Nucleari, NT 193 (92) Rev.1 Università Di Pisa Applications of Sys. Th. Codes to Nuclear Reactor Design and Accident Analysis 250. https://doi.org/10.13140/RG.2.2.32181.22241

Emonot, P., Souyri, A., Gandrille, J.L., Barré, F., 2011. CATHARE-3: A new system code for thermal-hydraulics in the context of the NEPTUNE project. Nuclear Engineering and Design S0029549311004018. https://doi.org/10.1016/j.nucengdes.2011.04.049

Equipe BETHSY, 1990. BETHSY General Description. Centre d'études nucléaires de Grenoble.

Hwang, M., Sim, S.K., Choi, K.-Y., Lee, K.W., 2019. Investigation of the Loop Seal Clearing Phenomena for the ATLAS DVI Line and Cold Leg SBLOCA Tests Using MARS-KS and RELAP5/MOD3.3. Nuclear Regulatory Commission.

Kumamaru, H., Briday, G., Kukita, Y., Juhel, D., Deruaz, R., 1992. LSTF and BETHSY counterpart tests on PWR small break LOCA, in: ANS Proc. of the 1992 National Heat Transfer Conf. pp. 285–292.

Muñoz-Cobo, J.L., Berna, C., Escrivá, A., 2018. Top-down scaling methodology from the LSTF facility to a three loop PWR plant applied to a SBLOCA event – The ROSA 1.2 test. Nuclear Engineering and Design 327, 248–273. https://doi.org/10.1016/j.nucengdes.2017.12.011

Préa, R., Fillion, P., Matteo, L., Mauger, G., Mekkas, A., 2020. CATHARE-3 V2.1: The new industrial version of the CATHARE code. Advances in Thermal Hydraulics 13. https://dx.doi.org/10.13182/ATH2020-31587

The ROSA-V Group, 1985. ROSA-IV Large Scale Test Facility (LSTF) System Description. JAERI-M 84237, Tokai-Mura, Japan.

Wilson, G.E., Boyack, B.E., 1998. The role of the PIRT process in experiments, code development and code applications associated with reactor safety analysis. Nuclear Engineering and Design 186, 23–37. https://doi.org/10.1016/S0029-5493(98)00216-7

Wulff, W., Zuber, N., Rohatgi, U.S., Catton, I., 2009. Application of Fractional Scaling Analysis to Loss of Coolant Accidents, System Level Scaling for System Depressurization. Journal of Fluids Engineering 131, 081402. https://doi.org/10.1115/1.3155994

Zuber, N., 1991. A hierarchical, Two-tiered Scaling Analysis, Appendix D of An Integrated Structure and Scaling Methodology for Severe Accident Technical Issue Resolution, in: NUREG/CR-5809. p. 688.

Zuber, N., Rohatgi, U.S., Wulff, W., Catton, I., 2007. Application of fractional scaling analysis (FSA) to loss of coolant accidents (LOCA). Nuclear Engineering and Design 237, 1593–1607. https://doi.org/10.1016/j.nucengdes.2007.01.017

Zuber, N., Wilson, G.E., Ishii, M., Wulff, W., Boyack, B.E., Dukler, A.E., Griffith, P., Healzer, J.M., Henry, R.E., Lehner, J.R., Levy, S., Moody, F.J., Pilch, M., Sehgal, B.R., Spencer, B.W., Theofanous, T.G., Valente, J., 1998. An integrated structure and scaling methodology for severe accident technical issue resolution: Development of methodology. Nuclear Engineering and Design 186, 1–21. https://doi.org/10.1016/S0029-5493(98)00215-5